CHARACTERIZING THE ANISOTROPIC QUARK GLUON PLASMA

A thesis submitted for the degree of

DOCTOR OF PHILOSOPHY (Science)

in

Physics (Theoretical)

by

MAHATSAB MANDAL

Department of Physics

UNIVERSITY OF CALCUTTA

August, 2016

Characterizing The Anisotropic Quark Gluon Plasma

Abstract

Formation and observation of a quark gluon plasma (QGP) in relativistic collisions between heavy nuclei is a primary goal of modern nuclear physics. In this thesis, we study the behavior the QGP which is anisotropy in momentum space. We investigate how big of a role plasma instability can play in the wake behavior and collective modes of a QGP. In the first work, we investigate the wake in charge density as well as the wake potential induced by a fast parton propagating through the anisotropic QGP. We find that the oscillatory behavior of the wake is amplified with the strength of the anisotropy when the parton moves parallel to the anisotropy direction whereas it diminishes for the perpendicular case. The investigation of the wake potential is extended to include a Bhatnagar-Gross-Krook (BGK) collisional kernel. In a collisional anisotropic QGP, the oscillatory behavior of the wake potential is smeared out. In anisotropic media, the effect of the jet of particles on the collective modes of a QCD plasma is studied.

To study the early time momentum space anisotropy, we need some observables, which are sensitive to the anisotropy in the quark and gluon distribution functions. The effect of time dependent momentum space anisotropy on the nuclear modification factor ($R_{\rm AA}$) is discussed. In the subsequent work, we have investigated the thermally averaged gluon-J/ψ dissociation cross section in the anisotropic system. We also calculate the survival probability of J/ψ by taking into account the initial state momentum space anisotropy. Finally, we study the space-time structure of the anisotropic QGP formed in heavy-ion collision by studying the two photon momentum correlation.

Mahatsab Mandal
Kolkata, India.

To My Uncle, Aunt and My Mother

For everything. Forever.

"Live for yourself and you will live in vain;
Live for others, and you will live again."
Bob Marley

DECLARATION

I, hereby declare that the investigation presented in the thesis has been carried out by me. I have adequately cited and referenced the original sources. The work is original and has not been submitted earlier as a whole or in part for a degree/diploma at this or any other Institution/University.

Mahatsab Mandal
Kolkata, India.

ACKNOWLEDGEMENTS

I first would like to express my deepest gratitude to my supervisor, Prof. Pradip K. Roy of Saha Institute of Nuclear Physics for his patient guidance and heart-warming care. His thoughtful and well-informed suggestions lead this thesis up to one of fruitful researches in nuclear physics. He taught me how to question thoughts and express ideas. This work would not have been possible without his guidance, support and encouragement.

I have no ward to thank Late. Prof. Abhee K. Dutt-Mazumder whose assistance, advice all through these years influence me a lot. His irrepressible courage and conviction will always inspire me, and I hope to continue to work with his noble thoughts.

It is my great pleasure to thank Prof. Sunanda Banerjee (SINP), Prof. Sukalyan Chottopadhyay (SINP), Prof. Sourav Sarkar (VECC), Prof. Jan e Alam (VECC), Prof. Nikhil Chakraborty (SINP) for their encouragement, support during my research. I would also like to thank Prof. Palash Baran Pal, Prof. Janaki Sita Mylavarapu, Prof. Parthasarathi Majumdar, Prof. Partha Mitra for their encouragement, support and teaching during my Post-M.Sc course work at SINP.

My special thanks to my senior lab mate Lusakadi for her help in my Ph.D Period. I would also like to thanks Sreedi, Jamildi, Payaldi, Kausikda, Biswarup, Souvik for their valuable comments and useful suggestions on the publication and my presentations. I am really fortunate to get the best opportunity to work with such talented people at SINP. I would like to express great thanks to my senior colleagues Subhroda, Subhojitda, Tapanda, Raktimda, Arindamda(comrade), Kushalda, Nazirda, Pabitrada whose ideas and support helped me a lot during my research work.

I would also like to thank my Post-M.Sc batch-mates of SINP, in particular Abhishek Chowdhury, Ujjal Gayan, Palash Khan, Anisur Rahaman, Sourish Bondyopadhyay, Abhishek Majhi, Anirban Biswas for their various academic and non-academic support. I would also like to extend huge, warm thanks to my my best friends Prosenjit whose con-

stant support helped me a lot in my Ph.D days. I would like to acknowledge my junior lab mates Kalyanmoy, Atanu, Sourav, Kuntal, Subhankar, Ashim, Biswarup, Niyaz and Argha for their helpfulness during my research work.

I am also thankful to Amit, Aminul, Rajani, Arnab, Samik, Rajarshi, Rajendra,Prithwish, Baishalidi, Subirda, Arindamda and Shyamalda. I am surely thankful to Dubey ji, Ashisda, Bijoyda, Lipydi, Dipankarda, Sudamda, Sanjibda, Pappuda, Sureshda, Saktida and Kartikda for their non-academic support.

I would also like to thank my colleagues of Hooghly Mohsin College and Govt. General Degree college at Kalna-I, in particular Anisurda, Goutamda, Goutamda(Dey), Manojda, Sanjibda, Arijitda, Manida, Saikat, Monohhar, Tanmoy and Rakhidi, for their encouragement and helpfulness during the last one year of my research.

I would like to acknowledge the Department of Atomic Physics, India for providing the financial support during the period of research. Thanks to library staff of our institution.

My sincere gratitude goes to my parents and my sister for their enormous support, cheering me up at all times.

Last but not least, I would like to pay high regards to my uncle Amal Kanti Mandal and my aunt Jharna Mandal for their patience, encouragement and inspiration throughout my research work and lifting me uphill this phase of life. Without their blessing I am incomplete.

Mahatsab Mandal

Kolkata, India.

Characterizing The Anisotropic Quark Gluon Plasma

Abstract

Formation and observation of a quark gluon plasma (QGP) in relativistic collisions between heavy nuclei is a primary goal of modern nuclear physics. In this thesis, we study the behavior the QGP which is anisotropy in momentum space. We investigate how big of a role plasma instability can play in the wake behavior and collective modes of a QGP. In the first work, we investigate the wake in charge density as well as the wake potential induced by a fast parton propagating through the anisotropic QGP. We find that the oscillatory behavior of the wake is amplified with the strength of the anisotropy when the parton moves parallel to the anisotropy direction whereas it diminishes for the perpendicular case. The investigation of the wake potential is extended to include a Bhatnagar-Gross-Krook (BGK) collisional kernel. In a collisional anisotropic QGP, the oscillatory behavior of the wake potential is smeared out. In anisotropic media, the effect of the jet of particles on the collective modes of a QCD plasma is studied.

To study the early time momentum space anisotropy, we need some observables, which are sensitive to the anisotropy in the quark and gluon distribution functions. The effect of time dependent momentum space anisotropy on the nuclear modification factor ($R_{\rm AA}$) is discussed. In the subsequent work, we have investigated the thermally averaged gluon-J/ψ dissociation cross section in the anisotropic system. We also calculate the survival probability of J/ψ by taking into account the initial state momentum space anisotropy. Finally, we study the space-time structure of the anisotropic QGP formed in heavy-ion collision by studying the two photon momentum correlation.

List Of Publications

Thesis Publications:

1. **Wake in anisotropic quark-gluon plasma**
   Mahatsab Mandal, Pradip Roy.
   Phys. Rev. D **86** (2012) 114002.
   Preprint : Nucl-th/1310.4657.

2. **Wake potential in collisional anisotropic quark-gluon plasma**
   Mahatsab Mandal, Pradip Roy.
   Phys. Rev. D **88** (2013) 074013.
   Preprint : Nucl-th/1310.4660.

3. **Jet-induced collective modes in an anisotropic quark-gluon plasma**
   Mahatsab Mandal, Pradip Roy.
   Phys. Rev. D **89** (2014) 074016.

4. **Nuclear modification factor in an anisotropic Quark-Gluon-Plasma**
   Mahatsab Mandal, Lusaka Bhattacharya, Pradip Roy.
   Phys. Rev. C **84** (2011) 044910.
   Preprint : Nucl-th/1101.5855.

5. **Gluon dissociation of J/ψ in anisotropic Quark-Gluon-Plasma**
   Mahatsab Mandal, Pradip Roy.
   Phys. Rev. C **86** (2012) 024915.
   Preprint : Nucl-th/1105.5528.

6. **Two Photon Correlation in Anisotropic Quark-gluon plasma**
   Payal Mohanty, Mahatsab Mandal, Pradip Roy.

Phys. Rev. C **89** (2014) 054915.

Preprint : Nucl-th/1305.5702.

Other Publications:

1. **Effect of running coupling on photon emission from quark-gluon plasma**

   Mahatsab Mandal, Pradip Roy, Sukanya Mitra, Sourav Sarkar.

   Phys. Rev. C **85** (2012) 067901.

   Preprint : Nucl-th/1205.0760.

2. **Systematic study of charmonium production in p-p collisions at LHC energies**

   Biswarup Paul, Mahatsab Mandal, Pradip Roy. Sukalyan Chattapadhyay.

   J. Phys. G **42** (2015) 065101.

   Preprint : Nucl-th/1411.6783.

3. **Pionic dispersion relations in the presence of a weak magnetic field**

   Souvik Priyam Adhya, Mahatsab Mandal, Subhrajyoti Biswas, Pradip Roy.

   Phys. Rev. D **93** (2016) 0749033.

   Preprint : Nucl-th/1601.04578.

Review

1. **Some Aspects of Anisotropic Quark-Gluon Plasma**

   Mahatsab Mandal, Pradip Roy.

   Adv. High. Energy Phys. **2013** (2013) 371908.

Conference Proceedings:

1. **Wake in anisotropic quark-gluon plasma**

   Mahatsab Mandal, Pradip Roy.

   DAE Symp.Nucl.Phys. **57** (2012) 810.

Axiv Submission:

1. **Energy Loss due to field fluctuations in a two-stream QCD Plasma**
   Mahatsab Mandal, Sreemoyee Sarkar, Pradip Roy.
   Preprint : Nucl-th/1109.1181.

2. **Effect of thermalized charm on heavy quark energy loss**
   Souvik Priyam Adhya,Mahatsab Mandal, Sreemoyee Sarkar, Pradip K. Roy, Sukalyan Chattapadhyay.
   Preprint : Nucl-th/1408.6705.

3. **Effect of anisotropy on HBT radii using lepton pair interferometry**
   Payal Mohanty, Mahatsab Mandal, Pradip K. Roy.
   Preprint : Nucl-th/1411.2322.

4. **Jet-dilepton conversion from an anisotropic quark-gluon plasma**
   Argha Mukherjee Mahatsab Mandal, Pradip Roy.
   Preprint : Nucl-th/1604.08313.

Notation and Conventions

Throughout this thesis we shall use the following conventions.. The matric tensor used is $g^{\mu\nu} = \text{diag}(1, -1, -1, -1)$. Most of the notation is introduced during the discussion and the frequently used notations are enlisted below:

$N - N$	Nucleon-Nucleon
$p - p$	proton-proton
$p - A$	proton-Nucleus with mass number A
$A - A$	Nucleus-Nucleus with mass number A
y	Particle rapidity ($= \frac{1}{2} \ln \left[\frac{E+p_z}{E-p_z}\right]$)
η	Space-time rapidity ($= \tan^{-1}(t/z)$), thus $t = \tau \cosh \eta$ and $z = \tau \sinh \eta$
p_T	transverse momentum
ξ	anisotropic parameter
p_{hard}	average momentum in the partonic distribution function
$\hat{n}$	direction of the anisotropy
τ_i	formation time
τ_{iso}	isotropization/thermalization time
T_i	initial temperature
T_c	Transition temperature
T_f	Thermal freeze-out temperature
ν	collisional rate
Γ	growth rate
m_D	Debye mass
d^4x	four-volume

Contents

Chapter 1

Introduction

The interaction between quarks (anti-quarks) is described by Quantum Chromodynamics (QCD) which is a non-abelian gauge theory. Quark (anti-quarks) are the elementary particles in the theory and interact with each other through the exchange of colored gluon. In QCD vacuum, the effective coupling constant decreases logarithmically as the momentum transfer increases as shown in Fig. 1.1. For large distance and small value of the four momentum, the interaction becomes strong between quarks, and hence, they remain confined within the hadron. This is known as quark confinement according to which the color charged particles cannot be found in free state. On the other hand, the small value of the coupling constant implies 'weak' interaction and quarks behave like free particles. This phenomena is known as "asymptotic freedom" [1, 2]. In this regime, the perturbative QCD (pQCD) approach can be applied to make predictions for observables expressed in terms of power of the coupling constant. According to lattice QCD (lQCD) at high temperature and/ or density QCD matter undergoes a phase transition that restores the broken symmetries and quarks and gluons can traverse freely over the dimension larger than 1 fm, typical size of hadrons. Therefore, a new state of matter composed of quarks and gluons in a deconfined state [3, 4, 5, 6, 7] is then possible. This new phase is known as quark gluon plasma (QGP).

Ultra-Relativistic heavy-ion collisions offer the unique opportunity to probe highly ex-

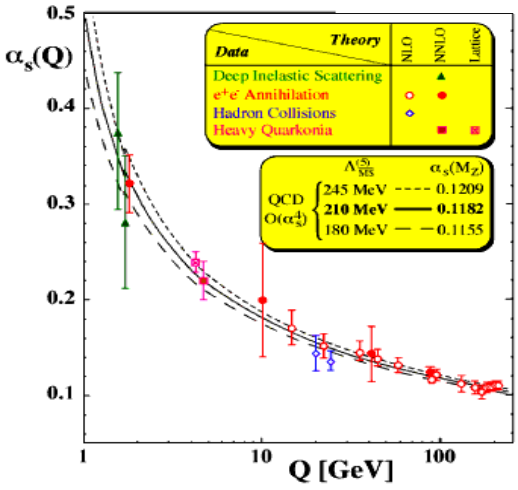

FIG. 1: QCD running coupling constant

Figure 1.1: *The summery of α_s measurements as a function of respective energy scale Q.*

ited hot and dense nuclear matter under controlled laboratory conditions [8]. Over the past three decades, the Relativistic Heavy-Ion Collider (RHIC) at Brookhaven National Laboratory (BNL) and the Large Hadron Collider (LHC) at European Center for Particle Physics (CERN) have succeeded to measure a wide spectrum of observables with heavy-ion beam. These observations suggest that a novel form of matter has been created in such experiments. The new state of partonic matter called QGP, is believed to exist in the early universe just micro-second after the Big-Bang [9] with zero baryon density. It is possible that neutron stars, in which the net baryon density exceeds the critical value of the phase transition [10], might contain a QGP at their core.

To estimate when the restoration of chiral symmetry breaking and a transition from hadronic matter to a Quark Gluon Plasma takes place, one can calculate the pressure and energy density in the vacuum that confines quarks and gluons which are weekly interacting inside the hadron and in the QGP. According to MIT bag model [11, 12, 13], when the pressure in the QGP and in a hadron gas becomes equal, a phase transition occurs. The sharp rise of energy density occurs at critical temperature $T_c \approx 170$ MeV for two active

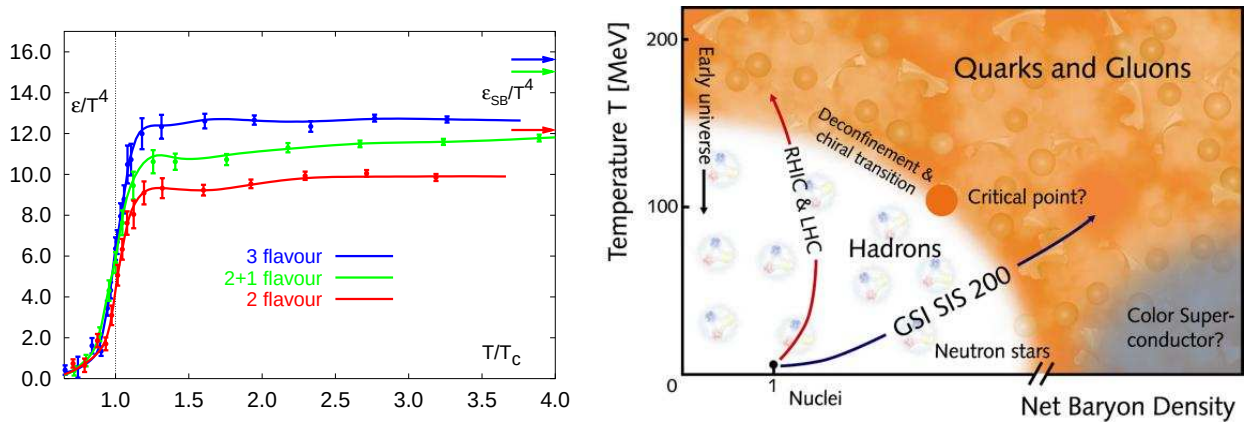

Figure 1.2: *Left: The energy density as a function of temperature from lattice QCD [17]. Right: A schematic phase diagram of QCD matter.*

light flavors (u and d) [14, 15]. At zero quark chemical potential or equivalently if the energy density of nuclear matter is raised above 1 GeV/fm^3 [16]. To obtain more accurate knowledge, this requires lQCD calculation [17]. Lattice QCD results, clearly shows a rapid rise of the energy density of the strongly interacting matter when the temperature $T \simeq T_c =$ 160 MeV, as shown in the left panel of Fig. 1.2. Such rapid rise at that temperature can be understood as a change in the degrees of freedom between confined matter and deconfined matter. However, such studies are performed for zero baryon-chemical potential ($\mu_{\rm B}$), i.e., for equal number of baryon and anti-baryon. The complete description of the QCD phase diagram is still unknown. A schematic view of the QCD phase diagram in the (T, μ_B) plane is shown in the right panel of Fig. 1.2. At low temperature and small value of the baryon-chemical potential ($\mu_{\rm B}$) the system is in hadronic phase. At low temperature and high $\mu_{\rm B}$, a phase transition occurs to color-superconducting phase. On the other scenario, i.e., for high temperature and low $\mu_{\rm B}$, the quark and gluon are deconfined and the chiral symmetry is restored [18].

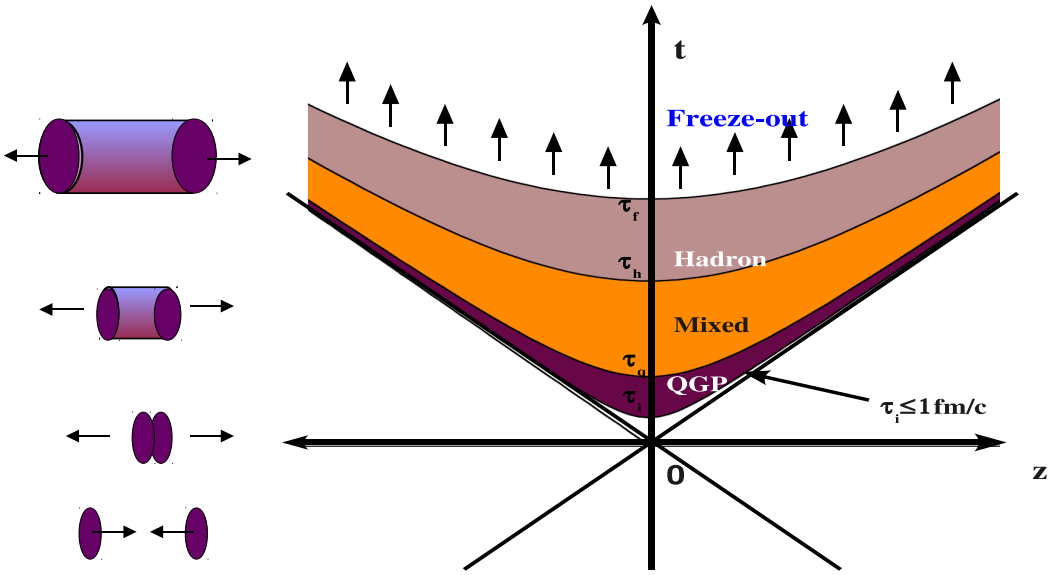

Figure 1.3: *Space-time diagram in heavy-ion collisions.*

1.1 QCD matter in Heavy Ion Collisions

In a heavy-ion collider, two beams of heavy ion are collided with velocity closer to the speed of light and create a "Little Bang" in the laboratory. In the center of mass frame of colliding nuclei, nuclei are contracted in the beam direction like pancakes due to Lorentz contraction. In the very early stage of the heavy-ion collision, high energetic particles are produced by initial hard scatterings which can be calculated by pQCD model. Initially the system is in pre-equilibrium phase. After the pre-equilibrium stage, the system comes into thermal equilibrium at initial time $\tau_{\rm i} = 0.1 - 1.0$ fm/c [19] due to the multiple scatterings among the initial partons. However, it is difficult to determine the value of $\tau_{\rm i}$. At the RHIC and LHC energies, the thermalized medium is expected to be at sufficiently high temperature. This medium would be in quark gluon plasma phase. Afterwards, the system start to expand due to huge pressure gradients and consequently it cools. If the first order phase transition is assumed, a mixed phase is expected to exist in which quarks and gluons begin to confine into the hadronic matter at the critical temperature T_c. When the system

cools further, all the quark matter are transformed into hadronic phase. After some time, when the mean free path of the hadrons exceeds the dimension of the system the hadrons freeze out and reach to the detector. The space-time evolution of heavy-ion collision is depicted in Fig 1.3.

1.2 Signature of QGP

In order to detect and studying such exotic state of matter, one needs some clear experimental signatures of its formation and/ or decays. One serious problem in detection of the QGP is its small size and very short life time. Therefore, direct detection of such state of matter is not possible. Furthermore, each stage of space-time evolution has specific characteristics regarding the particle production and lifetime. Therefore, the challenge both for theoretically and experimentally is to study of the signatures that are sensitive to the collision dynamics. During the last few decades, detection of QGP in heavy-ion collision has received significant attention and numerous signals have been proposed to probe the properties of such novel state of matter. Few such successful attempts have been discussed below.

1.2.1 Jet Quenching

High-energy partons behave as hard probes which are produced in the early stage of the collision due to hard scattering. In the heavy-ion collision experiments, the jets are created in pairs and propagate in opposite direction. If a pair of jets is created at the edge of the fireball, one of the jets will travel to the detector without interaction with the medium whereas the other jet will travel through the medium. While propagating through the QGP, the high energetic jet loses energy by collisional (interacting with the thermal quark and gluon) and radiative processes (bremsstrahlung). As a consequence, in the direction of propagation of the jet one observes a decrease of high energy hadrons. This phenomena is well known as jet quenching [20, 21, 22, 23, 24, 25, 26, 27]. The suppression of particles

with high p_T in the QGP is measured through the nuclear modification factor R_{AA}, the ratio of the measured jet yield in A + A collision relative to the expected yield from the binary scaled hadron-hadron collision. The reduction of the nuclear modification factor is seen in RHIC [28, 29] and LHC [30, 31] experiments and indicates the presence of the medium effect.

1.2.2 J/ψ Suppression

Suppression of J/ψ in $A + A$ collision relative to $p + p$ or $p + A$ collision is considered as a signature of chiral symmetry restoration [32, 33]. J/ψ particles are the bound state of $c\bar{c}$ pair dominantly produced by the fusion of gluons, Due to the heavy mass of the charm quark ($m_c \sim 1.5$ GeV), they are likely to be produced in the initial stage of the heavy-ion collision mainly from the hard scattering. In the QGP environment, binding of $c\bar{c}$ into a J/ψ is suppressed due to the Debye screening of color charges. The inclusive production of J/ψ is suppressed by a factor of $3 - 5$ at Super Proton Synchrotron (SPS) [34], RHIC [35] and LHC [36]. Thus, J/ψ suppression is a very powerful signature of the QGP formation.

1.2.3 Strangeness Enhancement

First, Rafelski and Hagedorn [37, 38] proposed that strangeness could be a useful signal for QGP formation in the heavy-ion collision experiments. Strange quarks are produced in the collision by interaction of two gluons ($gg \rightarrow s\bar{s}$) and annihilation of quark and anti-quark ($q\bar{q} \rightarrow s\bar{s}$). At high temperature, $T \geq 160$ MeV, the strangeness abundance saturates in the plasma in a very short time $\sim 10^{-23}$ sec and will lead to an enhanced production of strange and multi-strange particles. This kind of enhancement was observed for strange hyperons like Λ, Σ, Ω in nucleus- nucleus collisions compared to small interacting systems like proton-nucleus collisions [39].

1.2.4 Electromagnetic Probes

The advantage of photons, as well as dileptons is that these, once produced, can leave the interaction zone without much distortion in their energy and momentum. They carry the information of the collision dynamics very effectively which makes them a valuable tool of the early stage of the heavy-ion collision. Photons and dileptons are produced throughout the entire stages of the evolution of the collisions and their production cross-section depends on temperature.

Photons [4, 40, 41, 42, 43, 44, 45, 46, 47, 48, 49, 50, 51, 52] are produced in the early stage of the collision through the Compton ($q(\bar{q})g \rightarrow q(\bar{q})\gamma$) and annihilation ($q\bar{q} \rightarrow g\gamma$) processes. These are called prompt photons. This contribution can be accurately estimated by pQCD calculation. There are also photons from thermalized QGP, hadronic reaction and hadronic decays. To extract the thermal photons from QGP prompt photons, decay photons and photons from hadronic reaction have to be subtracted. Note that, the hard photon is dominated by the high p_T part of the momentum spectra, and decay photons populate to the low p_T part and intermediate domain of p_T spectra $\sim$ $1-3$ GeV are dominated by thermal photons. So, there is a small p_T window, i.e., $p_T \sim 2-5$ GeV [53], which may help in learning the properties of QGP.

The main source of thermal dileptons [54, 55, 56, 57, 58, 59, 60] from the QGP and hadronic sector are $q\bar{q}$ and $\pi^+\pi^-$ annihilation processes respectively. Also in the high mass region, there is the contribution from Drell-Yan (DY) process which can be calculated from pQCD. One can expect that thermal lepton pair production from QGP dominates in the mass range of $\sim 2-4$ GeV. It is important to mention that the window in the low-mass region will get populated by the other sources of dilepton production, mainly from the bremsstrahlung. This, among other reasons, makes the task extremely difficult for using it as a signature of QGP in this range. Thus the choice of high mass region is more suitable for QGP detection. Therefore, once we know their contribution we can subtract DY contribution from the total yield to get the thermal production yield.

1.3 Thermalization and Plasma Instability

In relativistic heavy-ion collision at RHIC one of the most breathtaking observation was the strong collective behavior of the matter which is evident from the elliptic flow measurements [61]. When two heavy nuclei collide, the center of the two nuclei are at a distance b, where b is the impact parameter. Due to non-central heavy-ion collision, the initial energy density is not azimuthally isotropic. As flow follows from the energy density gradient, it will be stronger along the short overlap direction (in-plane) than along the long overlap direction (out-of-plane), which leads to an azimuthal momentum space anisotropy of the particle emission in the plane transverse to the beam direction. The azimuthal anisotropy is quantified by defining the elliptic flow parameter, v_2 as [62]

$$v_2 = < \frac{p_X^2 - p_Y^2}{p_X^2 + p_Y^2} > . \tag{1.1}$$

In ideal hydrodynamics model, the stress energy tensor ($T^{\mu\nu}$) is isotropic in momentum space, i.e., the components $T_{ij} = p\delta_{ij}$, $T^{00} = \epsilon$ and $T^{0i} = 0$, where p is the pressure and ϵ is the energy density of the matter. Ideal hydrodynamical models have been able to fit the low p_T dependence of the elliptical flow v_2, which leads to strong evidence that the matter created in the heavy-ion collision becomes isotropic and thermalized and the thermalized time approximately is $\tau_{\rm iso}(\tau_{\rm therm}) = 0.5 - 1.0$ fm/c after the collision [63, 64]. On the contrary, pQCD calculation shows slower thermalization [65]. Such a fast thermalization can be possible for strongly coupled QGP [66]. However, recent hydrodynamical studies [67] that include the effect of shear and bulk viscosities have shown that RHIC data does not require a short thermalization time. The non-zero viscosities modifies stress energy tensor. As a result, RHIC data shows that even thermalization time $\tau_{\rm iso} \sim 2$ fm/c can reproduce the elliptical flow data quite well [31]. Moreover, recent transport theory assumes parton interaction to be responsible for the thermalization of 'weakly' coupled plasma and leads to the longer thermalization time. In the "bottom-up" scenario, for binary collision processes ($2 \rightarrow 2$), a relatively long time is required for the approach to kinetic equilibrium,

whereas inclusion of $2 \rightarrow 3$ pQCD bremsstrahlung process speeds up the equilibration significantly [65].

Due to the poor knowledge of the initial conditions of the plasma there is sizable amount of uncertainty in the estimate of thermalization time. Non-equilibrium gauge field dynamics plays an important role in the equilibration process of the plasma [68, 69, 70, 71, 72, 73]. In these approaches the QGP is assumed to be homogeneous and stationary but anisotropic in momentum space. Kinetic instability can occur due to the interaction of the plasma and the jet parton which leads to electric or magnetic instabilities. Plasma instability could be an explanation of the fast isotropization predicted by the study of elliptic flow at RHIC data [74, 75].

At the early stage, of the heavy-ion collision, the system expands along the beam direction. If the matter expands along the beam direction too quickly, there will not be enough time for the constituents to interact and therefore the system will not reach thermal equilibrium. Longitudinal expansion of the matter causes the system to quickly become much colder in the longitudinal direction than in the transverse direction. As a result, initially the longitudinal expansion rate is larger than the parton interaction rate which leads to momentum space anisotropy in the $p_T - p_L$ plane, corresponding to $< p_L^2 > << < p_T^2 >$ in the local rest frame. One can then ask how long it would take for interaction to restore isotropy in the $p_T - p_L$ plane. In the "bottom-up" scenario [65], it addresses the dynamics of hard modes (particles) coupled to the soft modes (field) which causes the system to become isotropic.

The plasma instability plays an important role in the thermalization process of the QGP. In presence of the pre-equilibrium momentum space anisotropy, one can find that soft modes with momentum $k << gT$, where g is the coupling constant and T is the temperature of the system, is initially unstable. The characteristic inverse time of instability development is roughly of the order of gT, whereas the inverse equilibration time is of order $g^4 \ln(g)T$ for binary collisions. As a result, in the weak coupling limit, the dynamics of an anisotropic

QGP is dominated by the growth rate of the unstable modes. These unstable modes grow exponentially with time which leads to a more rapid thermalization and isotropization of the soft modes in QGP. Such processes may play an active role in the dynamical properties of the QGP.

1.4 Organization of the Thesis

The thesis is organized as follows. In Chapter 2, we shall discuss the kinetic theory for QCD plasma and present a formalism of the non-Abelian Vlasov equations for QCD constituents. There is a possibility that the QGP may be anisotropic in momentum space after the formation. In this chapter we briefly review the phenomenological models of anisotropic plasma and discuss the collective modes of an anisotropic QGP.

In Chapter 3, we investigate the impact of the pre-equilibrium momentum anisotropy on the wake in QCD plasma. The experimental azimuthal dihadron distribution at RHIC shows a double peak structure in the away side [76, 77] for the intermediate p_T particles. Such peak were predicted as a signature of Mach shocks developed by the passage of jets propagating through the plasma. Moreover, the partonic jets propagating through the QGP created in the heavy-ion collision leads to the formation of the wakes. These wakes are proposed as possible explanation for the double peak structure in the away side for the intermediate p_T particles. The wake behavior is concerned with the screening behavior of the moving parton. We extend this study to a pre-equilibrium momentum space anisotropic plasma and discuss, in detail, the induced charge density and wake potential in an anisotropic QGP. In addition, we calculate wake potential within the framework of the Boltzmann transport equation with a Bhatnagar-Gross-Krook (BGK) collisional kernel.

In chapter 4, we investigate the characteristics of collective modes induced by relativistic jet in a collisionless anisotropic QGP. When stream of particles interact with the plasma, plasma instabilities develope, leading to initial stage of fast growth of the gauge field. In studying the evolution of such system, we use the method of the plasma physics within

the framework of the quark-gluon transport theory in the weak coupling region, $g << 1$. We have neglected hard mode interaction and they are treated as (quasi-) particles which propagate in the background of the soft modes, acting as classical gauge field.

The impact of pre-equilibrium momentum anisotropy on various observables which are sensitive to the collision dynamics in the early stage of the heavy-ion collisions is discussed in Chapter 5. Chapter 6 contains the summery and outlook.

• ○ •

Chapter 2

KINETIC THEORY OF QUARK-GLUON PLASMA

Kinetic theory is introduced as the guiding principles with which to build the effective theory for the soft modes of hot/dense matter produced in the heavy-ion collisions. At the early stage of the collision, the temperature T of the system is high enough such that the plasma is rather weakly coupled i.e. running coupling $g(T) << 1$. In this weak coupling regime, the plasma particle, i.e., the quarks and gluons have momentum scale $k \sim T$ and typical thermal wavelength $\lambda_T = 1/k$ [78, 79]. The effect of the interaction on the particle motion depends both on the gauge field and the wavelength of the modes under study. In the hard degrees of freedom, the gauge field fluctuations produce a small perturbation on the particle motion unless the field is very large, i.e., unless $A \sim T/g$. But for the case of plasma particles with momentum $k \sim T$, it is found that $A \sim T$ [80].

The collective motion of individual particles appears on a space-time scale $\lambda \sim 1/(gT)$. This scale appears as the energy of the quasi-particles. The thermal fluctuations at the scale $gT << T$ is known as the *soft* scale. At this scale the magnitude of the field fluctuations is $A \sim \sqrt{g}T$ and derivatives are of the order $\partial_x \sim gT$. In case of soft modes, the field fluctuation is much higher than the kinetic term. So, at the momentum scale $k \sim gT$ the soft modes are still perturbative. The fact that the characteristic wavelength of the collective excitation is larger than the thermal wavelength suggests that these collective

effects can be described by Vlasov type Kinetic equation [80, 81]. Using the semi-classical kinetic equations one can derive the hard loop induced current paying much attention to the gauge aspects of the procedure. In this way, we explicitly demonstrate how the gluon polarization tensor can be obtained and how and it can naturally be extended to study the collective modes of the QGP.

In this chapter we will derive the color current and gluon self-energy using non-Abelian Vlasov equations. This leads to an effective theory for the collective modes at the scale gT for the isotropic plasma. We also derive both stable and unstable collective modes for the anisotropic system.

2.1 Classical Transport Theory for a Non-Abelian Plasma

The distribution functions of quantum colored particles are Hermitian $N_c \times N_c$ matrices whose dimensionality depends on the color representation of the particles. Quarks and antiquarks belong to the fundamental representation of $SU(3)_c$. The quark (antiquark) distribution function $Q(P,X)$ ($\bar{Q}(P,X)$) is a 3×3 matrix in color space. Here X denotes the space-time quark coordinate and P is its momentum. The distribution functions are not gauge invariant, but transforms under local gauge transformations as [80]

$$Q(P,X) \to U(X)Q(P,X)U^{\dagger}(X), \tag{2.1}$$

where $U(X)$ is the transformation operator in the fundamental representation.

The distribution function of gluons is a Hermitian $(N_c^2-1) \times (N_c^2-1)$ matrix in the adjoint representation of $SU(3)_c$. The gluon distribution function $\mathcal{G}(P,X)$ transforms under a local gauge transformation as

$$\mathcal{G}(P,X) = \mathcal{M}(X)\mathcal{G}(P,X)\mathcal{M}^{\dagger}(X) \tag{2.2}$$

where $\mathcal{M}_{ab}(X) = \mathrm{Tr}[\tau_a U(X)\tau_b U^{\dagger}(X)]$ with τ_a, $(a = 1, 2, ..., N_c^2-1)$ being the $SU(3)$ group generators in the fundamental representation.

The distribution functions of quarks, antiquarks and gluons satisfy the following kinetic equations [82, 83]:

$$\begin{aligned} P_\mu D^\mu Q(P,X) + \frac{g}{2} P^\mu \frac{\partial}{\partial P_\nu}\{F_{\mu\nu}(X), Q(P,X)\} &= C[f], \\ P_\mu D^\mu \bar{Q}(P,X) - \frac{g}{2} P^\mu \frac{\partial}{\partial P_\nu}\{F_{\mu\nu}(X), \bar{Q}(P,X)\} &= \bar{C}[f], \\ P_\mu \mathcal{D}^\mu \mathcal{G}(P,X) + \frac{g}{2} P^\mu \frac{\partial}{\partial P_\nu}\{\mathcal{F}_{\mu\nu}(X), \mathcal{G}(P,X)\} &= C_g[f]. \end{aligned} \tag{2.3}$$

where $\{...,...\}$ denotes the anticommutator, $D^\mu = \partial^\mu + ig[A^\mu, ...]$ is the covariant derivative in the adjoint representation of the color group. A_μ and $F_{\mu\nu}(= [D_\mu, D_\nu]/(ig))$ are the chromodynamic mean-field or background four potential and stress tensor respectively, where $A_\mu(X) = A^a_\mu(X)\tau^a$, $F_{\mu\nu}(X) = F^a_{\mu\nu}(X)\tau^a$. The covariant derivative is $\mathcal{D}^\mu = \partial^\mu - ig[\mathcal{A}^\mu, ...]$ with $\mathcal{A}^\mu$ and $\mathcal{F}^{\mu\nu}$ are defined as $\mathcal{A}^\mu_{ab}(X) = if_{abc}A^\mu_c(X)$ and $\mathcal{F}^{\mu\nu}_{ab}(X) = if_{abc}F^{\mu\nu}_c(X)$ respectively, where f_{abc} is the $SU(N_c)$ group structure constant. In Eqs.(2.3) C and $\bar{C}$ represent the collision terms. For time scales shorter than the mean free path time the collision terms can be neglected, as typically done in the so-called Vlasov approximation [68, 69, 84, 85, 86, 87, 88, 89, 90, 91].

A complete, self-consistent set of non-Abelian Vlasov equations for the distribution function and the mean color field is obtained by augmenting the Vlasov equation with the Yang-Mills equations

$$D_\mu F^{\mu\nu}(X) = J^\nu(X) = J^\nu_g(X) + J^\nu_q(X) \tag{2.4}$$

The total current $J^\nu(X)$ is given by the sum of contributions of gluon($J^\nu_g(X)$), quarks and antiquarks($J^\nu_q(X)$). It can easily be seen that the transport Eqs. (2.3) and Eq.(2.4) is gauge invariant. The color current is expressed in the fundamental representation as [71, 88]

$$\begin{aligned} J^\mu(X) &= -g\int \frac{d^3p}{(2\pi)^3 2E} P^\mu \Big[Q(P,X) - \bar{Q}(P,X) \\ &- \frac{1}{N_c}\mathrm{Tr}[Q(P,X) - \bar{Q}(P,X)] + 2i\tau_a f_{abc}\mathcal{G}_{bc}(P,X)\Big]. \end{aligned} \tag{2.5}$$

2.1.1 Linearized Transport Theory

We assume that the distribution functions which enter in the set of transport equations can be decomposed into regular and fluctuating components. Thus, the distribution functions of the plasma particles can be expressed as

$$\begin{aligned} Q_{ij}(P,X) &= n(\mathbf{p})\delta_{ij} + \delta Q_{ij}(P,X), \\ \bar{Q}_{ij}(P,X) &= \bar{n}(\mathbf{p})\delta_{ij} + \delta \bar{Q}_{ij}(P,X), \\ \mathcal{G}_{ab}(P,X) &= n_g(\mathbf{p})\delta_{ab} + \delta \mathcal{G}_{ab}(P,X). \end{aligned} \tag{2.6}$$

The quark(antiquark) and gluon distribution functions $n(\mathbf{p})(\bar{n}(\mathbf{p}))$ and $n_g(\mathbf{p})$ are Fermi-Dirac and Bose-Einstein distributions respectively. We also assume that

$$|n| >> |\delta Q| \quad \text{and} \quad |\bigtriangledown_p n| >> |\bigtriangledown_p \delta Q|. \tag{2.7}$$

Substituting Eqs.(2.6) in Eq.(2.5) we find the color current induced by the fluctuations as follows,

$$\begin{aligned} J^\mu(X) &= -g\int \frac{d^3p}{(2\pi)^3 2E} P^\mu \Big[\delta Q(P,X) - \delta\bar{Q}(P,X) \\ &- \frac{1}{N_c}\mathrm{Tr}[\delta Q(P,X) - \delta\bar{Q}(P,X)] + 2i\tau_a f_{abc}\delta\mathcal{G}_{bc}(P,X)\Big]. \end{aligned} \tag{2.8}$$

By substituting Eqs.(2.6) into the transport Eqs.(2.3), one can deduce the following expression of the linearized transport equations [88]:

$$\begin{aligned} P_\mu D^\mu \delta Q(P,X) &= -gP^\mu F_{\mu\nu}(X)\frac{\partial n(\mathbf{p})}{\partial P_\nu}, \\ P_\mu D^\mu \delta \bar{Q}(P,X) &= gP^\mu F_{\mu\nu}(X)\frac{\partial \bar{n}(\mathbf{p})}{\partial P_\nu}, \\ P_\mu \mathcal{D}^\mu \delta \mathcal{G}(P,X) &= -gP^\mu \mathcal{F}_{\mu\nu}(X)\frac{\partial n_g(\mathbf{p})}{\partial P_\nu}. \end{aligned} \tag{2.9}$$

Here, the stress tensor and δQ, $\delta\bar{Q}$ or $\delta\mathcal{G}$ are assumed to be of the same order.

To solve Eqs.(2.9) one can use the non-abelian parallel transporter or Wilson line

$$U(X,Y) = \mathcal{P}\exp\left[-ig\int_X^Y dZ_\mu A^\mu(Z)\right], \tag{2.10}$$

where $\mathcal{P}$ denotes the path ordering of the color matrices from X to Y. Using the parallel transporter one finds the solutions of Eqs.(2.9) as

$$\begin{aligned}
\delta Q(P,X) &= -g\int d^4Y\, G_p(X-Y)U(X,Y)P^\mu F_{\mu\nu}U(Y,X)\frac{\partial n(\mathbf{p})}{\partial P_\nu},\\
\delta \bar{Q}(P,X) &= -g\int d^4Y\, G_p(X-Y)U(X,Y)P^\mu F_{\mu\nu}U(Y,X)\frac{\partial \bar{n}(\mathbf{p})}{\partial P_\nu},\\
\delta \mathcal{G}(P,X) &= -g\int d^4Y\, G_p(X-Y)\mathcal{U}(X,Y)P^\mu \mathcal{F}_{\mu\nu}\mathcal{U}(Y,X)\frac{\partial n_g(\mathbf{p})}{\partial P_\nu},
\end{aligned} \tag{2.11}$$

where $G_p(X)$ is the Green's function of the kinetic operator which satisfies

$$P_\mu \partial^\mu G_p(X) = \delta^{(4)}(X) \tag{2.12}$$

and

$$G_p(X) = E^{-1}\Theta(t)\delta^3(x-\mathbf{v}t) \tag{2.13}$$

where $\mathbf{v}=\mathbf{p}/E$ is the parton velocity.

Combining Eqs.(2.11) and (2.8), the color current can be written as:

$$J^\mu(X) = g^2\int \frac{d^3p}{(2\pi)^3 2E}P^\mu P^\nu \int d^4Y\, G_p(X-Y)U(X,Y)F_{\mu\nu}U(Y,X)\frac{\partial f(\mathbf{p})}{\partial P_\nu}, \tag{2.14}$$

where $f(p)=N_f(n(\mathbf{p})+\bar{n}(\mathbf{p}))+2N_c n_g(\mathbf{p})$, N_f being the number of flavors. This equation can be solved using the Fourier transform. As we mentioned earlier, scales of interests are $A\sim\sqrt{g}T$ and $\partial\sim gT$, we neglect the terms which are not leading order in g and the theory becomes effectively Abelian as $D\to\partial$ and stress tensor $F^{\mu\nu}\to\partial_\mu A_\nu-\partial_\nu A_\mu$. Also, the parallel transporter U becomes unity. Within such an approximation one can perform a Fourier transform of the induced current in Eq.(2.8) to the momentum space to obtain

$$J^\mu(K) = g^2\int \frac{d^3p}{(2\pi)^3 2E}P^\mu \frac{\partial f(\mathbf{p})}{\partial P_\beta}\Big[g^{\beta\nu}-\frac{K^\beta P^\nu}{K.P+i\epsilon}\Big]A_\nu(K). \tag{2.15}$$

For sufficiently weak gauge field A^μ, the induced current $J^\mu(K)$ can be expressed as

$$J^\mu_a(K) = \Pi^{\mu\nu}_{ab}(K)A^b_\nu(K). \tag{2.16}$$

By functional differentiation one gets the polarization tensor as [88]

$$\Pi^{\mu\nu}(K) = g^2 \int \frac{d^3p}{(2\pi)^3 2E} P^\mu \frac{\partial f(\mathbf{p})}{\partial P_\beta} \Big[g^{\beta\nu} - \frac{K^\beta P^\nu}{K.P + i\epsilon} \Big] \tag{2.17}$$

In color space, the polarization tensor is proportional to a unit matrix. The only tensors that can appear in $\Pi^{\mu\nu}(K)$ are $g^{\mu\nu}$ and $K^\mu K^\nu$. The same result can be obtained in the diagrammatic approach using the HTL approximation with the assumption that the distribution function is symmetric under $\mathbf{p} \to -\mathbf{p}$ [88]. It is seen that this tensor is symmetric, $\Pi^{\mu\nu}(K) = \Pi^{\nu\mu}(K)$ and transverse, $K^\mu \Pi^{\mu\nu}(K) = 0$.

The effective theory for the soft modes can be expressed as covariant form of Maxwell equation

$$\partial_\mu F^{\mu\nu} = J^\mu_{\text{ind}} + J^\mu_{\text{ext}}, \tag{2.18}$$

with the external current J^μ_{ext}. By combining Eq.(2.16) and Eq.(2.18), it can be shown that the external current is related to the gauge field as

$$[K^2 g^{\mu\nu} - K^\mu K^\nu + \Pi^{\mu\nu}(K)] A_\nu(K) = -J^\mu_{\text{ext}}(K). \tag{2.19}$$

Due to the gauge invariance of the self-energy we can write the above equation in terms of a physical electric field by specifying a certain gauge. In the temporal axial gauge, where $A_0 = 0$, we obtain,

$$[(k^2 - \omega^2)\delta^{ij} - k^i k^j + \Pi^{ij}(K)] E^j = [\Delta^{-1}(K)]^{ij} E^j(K) = i\omega J^i_{ext}(K), \tag{2.20}$$

with

$$[\Delta^{-1}(K)]^{ij} = (k^2 - \omega^2)\delta^{ij} - k^i k^j + \Pi^{ij}(K). \tag{2.21}$$

The poles of the effective propagator $\Delta^{ij}(K)$ gives the dispersion relation for the waves in the medium. The above expression can also be written in terms of chromo-dielectric tensor $\epsilon^{ij}(K)$ as

$$[k^2 \delta^{ij} - k^i k^j - \omega^2 \epsilon^{ij}(K)] E^j = i\omega J^i_{ext}(K). \tag{2.22}$$

The dielectric tensor and the polarization tensor are related by the following relation [83, 91]:

$$\epsilon_{ij} = \delta_{ij} - \frac{\Pi^{ij}}{\omega^2}. \tag{2.23}$$

2.1.2 Collective modes in the isotropic plasma

As we have already seen, polarization tensor satisfies the transversality condition, which implies that only two components are independent and the general form can be written as

$$\Pi^{\mu\nu}(K) = \mathcal{P}_{\mu\nu}\Pi_T(K) + \mathcal{Q}_{\mu\nu}\Pi_L(K) \tag{2.24}$$

where the transverse and longitudinal projection tensors have the following forms:

$$\begin{aligned} \mathcal{P}_{\mu\nu} &= \tilde{g}_{\mu\nu} - \frac{\tilde{K}_\mu \tilde{K}_\nu}{\tilde{K}^2} \\ \mathcal{Q}_{\mu\nu} &= \frac{k^2}{\tilde{K}^2}\bar{u}_\mu \bar{u}_\nu \end{aligned} \tag{2.25}$$

Here,

$$\begin{aligned} \tilde{g}_{\mu\nu} &= g_{\mu\nu} - u_\mu u_\nu, \\ \tilde{K}_\mu &= K_\mu - \omega u_\mu, \\ \bar{u}_\mu &= u_\mu - \frac{\omega}{K^2}K^\mu, \\ \text{and } \tilde{K}^2 &= K^2 - \omega^2 = -\mathbf{k}^2 < 0. \end{aligned} \tag{2.26}$$

in which u_μ is the four velocity of the fluid with $u^\mu u_\mu = 1$. The tensor $\tilde{g}_{\mu\nu}$ and the four vector $\tilde{K}_\mu$ are orthogonal to u_μ. In the rest frame of the plasma, i.e., for $u_\mu = (1, 0, 0, 0)$, using the properties of the projection operators, one can obtain the scalar functions in Eq.(2.24) as

$$\begin{aligned} \Pi_L(K) &= -\frac{K^2}{k^2}\Pi_{\mu\nu(K)}, \\ \Pi_T(K) &= \frac{1}{2}[g^{\mu\nu}\Pi_{\mu\nu}(K) - \Pi_L(K)] \\ &= \frac{1}{2}(\delta_{ij} - \frac{k_i k_j}{k^2})\Pi_{ij}(K). \end{aligned} \tag{2.27}$$

which, for gluon, leads to

$$\Pi_T(K) = \frac{m_D^2}{2}\frac{\omega^2}{k^2}\Big[1-\frac{\omega^2-k^2}{2\omega k}\log\frac{\omega+k}{\omega-k}\Big], \tag{2.28}$$

and

$$\Pi_L(K) = m_D^2\Big[\frac{\omega}{2k}\log\frac{\omega+k}{\omega-k}-1\Big] \tag{2.29}$$

where m_D is the Debye mass and is given by

$$m_D^2 = -\frac{g^2}{2\pi^2}\int_0^\infty dp\, p^2\frac{df(\mathbf{p})}{df}. \tag{2.30}$$

In case of isotropic QCD plasma

$$m_D^2 = g^2T^2(\frac{2N_c+N_f}{6}) \tag{2.31}$$

for zero quark chemical potential. At finite chemical potential (μ), $m_D^2 = \frac{g^2}{\pi^2}(\mu^2+\frac{\pi^2T^2}{6}(2N_c+N_f))$. We can determine the dispersion relation of the isotropic system with the help of the effective propagator. Using the relation (2.21) we calculate the dispersion relation of transverse and longitudinal modes separately. The transverse dispersion relation is,

$$k^2-\omega_T^2+\Pi_T=0, \tag{2.32}$$

whereas for the longitudinal mode we have,

$$\omega_L^2-\Pi_L=0. \tag{2.33}$$

The transverse and the longitudinal modes are designated by ω_T and ω_L respectively. For $k\to 0$ we find $\omega_L(0)=\omega_T(0)=\sqrt{\frac{1}{3}m_D^2}=m_g$. The thermal gluon mass m_g is identical to the plasma frequency. For high momentum $k\to\infty$ we get $\omega_{L,T}(k\to\infty)=k$, obtaining the free dispersion relation. However for general k the Eqs.(2.32) and (2.33) have to be solved numerically and the solutions of the dispersion relation for the propagating transverse and longitudinal modes are displayed in Fig. 2.1. These propagating modes exist above

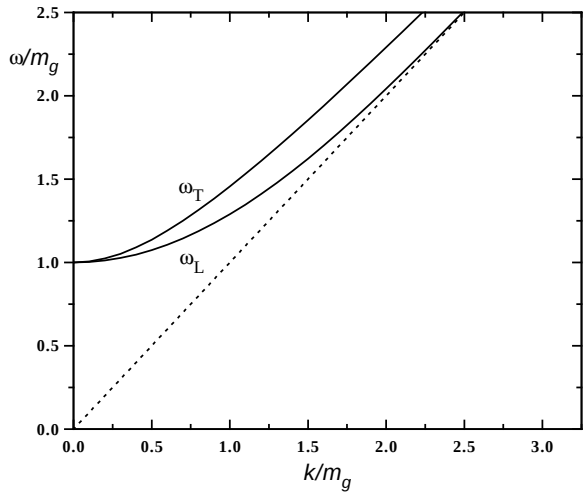

Figure 2.1: *Dispersion relation for transverse and longitudinal gluons modes.*

a common plasma frequency $\omega > \omega_{\rm pl} = \sqrt{m_D^2/3}$, which are always above the light cone ($\omega > k$) and are called normal modes. For $0 < \omega < \omega_{\rm pl}$, k becomes imaginary and there are no stable modes. However, there is a collective behavior which leads to the screening both in the magnetic and electric field as long as $\omega > 0$, which is known as the dynamical screening phenomenon [79].

2.2 The anisotropic Quark-Gluon Plasma

As mentioned earlier, shortly after the collision, the rapid expansion of the matter along the beam direction causes faster cooling in the longitudinal direction than the transverse direction, leading to the phase space distributions of plasma particles to be anisotropic in momentum space [67, 68, 71, 72, 74, 75, 88, 89, 90, 91, 92, 93, 94, 95, 96, 97, 98, 99, 100]. At some later time, the system returns to an isotropic state due to the effect of the parton interactions which overcome the plasma expansion rate. Therefore, it is interesting to investigate what effect the presence of momentum anisotropy has on the dynamics of the system and what differences one can expect when comparing to the usually studied isotropic

case.

In this section we will investigate the collective modes of QGP with momentum space anisotropy. In an isotropic system all the particles moves in all directions with equal probability. However, in a system with momentum anisotropy, there will be a preferred direction. The anisotropic distribution function can be obtained by stretching or squeezing an isotropic distribution function along a certain direction, thereby preserving a cylindrical symmetry in momentum space. We shall use the following ansatz [71, 95]:

$$f(\mathbf{p}) = f_\xi(\mathbf{p}) = \mathcal{N}(\xi) f_{\rm iso}(\sqrt{\mathbf{p}^2 + \xi(\mathbf{p}.\hat{\mathbf{n}})^2}, p_{\rm hard}), \tag{2.34}$$

for an arbitrary isotropic distribution function $f_{\rm iso}(|\mathbf{p}|)$ and $\hat{\mathbf{n}}$ is the direction of anisotropy. The parameter ξ is the degree of anisotropy ($-1 < \xi < \infty$) and is given by $\xi = \frac{1}{2}\frac{\langle p_T^2\rangle}{\langle p_z^2\rangle} - 1$. It is important to notice that $\xi > 0$ corresponds to a contraction of the distribution in the $\hat{\mathbf{n}}$ direction, whereas $-1 < \xi < 0$ corresponds to a stretching of the distribution in the anisotropic direction. The factor $\mathcal{N}(\xi)$ is the normalization factor. To fix $\mathcal{N}(\xi)$ we ensure that the overall particle number is same both for isotropic and arbitrary anisotropic systems and it is given by $\mathcal{N}(\xi) = \sqrt{1+\xi}$. Fig. 2.2 shows the Fermi-Dirac distribution in the presence of anisotropy. In this context, we assume that $\hat{\mathbf{n}}$ is in the direction of beam axis along which the system expands initially. $p_{\rm hard}$ is related to the average momentum in the partonic distribution function. In case of isotropic plasma, $p_{\rm hard}$ is related to the plasma temperature T.

2.2.1 Tensor Decomposition and Self-Energy Structure

We have already mentioned earlier that initially plasma expands only in one preferred direction and we can no longer decompose the self-energy into transverse and longitudinal parts. We therefore, need to construct a tensorial basis to represent the self-energy which depends not only on the momentum k^i but also depends on a fixed anisotropy vector n^i, with $n^2 = 1$. Using the proper tensorial basis[71] one can decompose the self-energy in

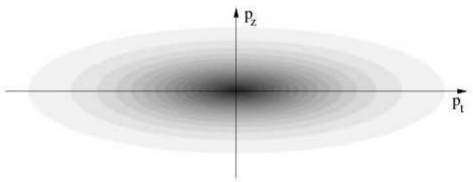

Figure 2.2: *Contour plot of a squeezed Fermi-Dirac distribution with anisotropy parameter* $\xi = 10$. *[101]*

terms of four structure functions as:

$$\Pi^{ij}(k) = \alpha A^{ij} + \beta B^{ij} + \gamma C^{ij} + \delta D^{ij}, \tag{2.35}$$

where

$$\begin{aligned} A^{ij} &= \delta^{ij} - k^i k^j/k^2, \\ B^{ij} &= k^i k^j/k^2, \\ C^{ij} &= \widetilde{n}^i \widetilde{n}^j/\widetilde{n}^2, \\ D^{ij} &= k^i \widetilde{n}^j + k^j \widetilde{n}^i, \end{aligned} \tag{2.36}$$

with $\widetilde{n}^i = A^{ij} n^j$ and it obeys $\widetilde{\mathbf{n}}.k = 0$ and $n^2 = 1$. We can determine the four structure functions by taking the following contraction:

$$\begin{aligned} k^i \Pi^{ij} k^j &= \mathbf{k}^2 \beta, \\ \tilde{n}^i \Pi^{ij} k^j &= \tilde{n}^2 \mathbf{k}^2 \delta, \\ \tilde{n}^i \Pi^{ij} \tilde{n}^j &= \tilde{n}^2 (\alpha + \gamma), \\ \mathrm{Tr}\Pi^{ij} &= 2\alpha + \beta + \gamma. \end{aligned} \tag{2.37}$$

All the four structure functions depend on the Debye mass (m_D), the frequency (ω), the momentum (k), the anisotropic parameter (ξ) and $\hat{\mathbf{k}}.\hat{\mathbf{n}} = \cos\theta_n$. In the isotropic limit, $\xi \to$

0, the structure functions γ and δ vanish and α and β are directly related to the transverse and longitudinal components of the polarization tensor of the plasma respectively:

$$\begin{aligned} \alpha(K,0) &= \Pi_T(K), \\ \beta(K,0) &= \frac{\omega^2}{k^2}\Pi_L(K), \\ \gamma(K,0) &= 0, \\ \delta(K,0) &= 0. \end{aligned} \tag{2.38}$$

where Π_T and Π_L are given by Eqs.(2.28) and (2.24). For finite ξ, analytic structure of the functions is the same as for Π_T and Π_L as in the isotropic case, namely there is a cut in the complex ω plane which can be chosen to run along the real ω axis from $-k < \omega < k$. For real valued ω the structure functions are real for $\omega > k$ which leads to Landau damping and imaginary for all $\omega < k$. For imaginary value of ω all four structure functions have real values.

Now we construct the effective propagator Δ^{ij} with the help of the structure functions. Inverse of the propagator, in terms of tensor basis is obtained using Eq.(2.21)

$$\Delta^{-1}_{ij}(K) = (k^2 - \omega^2 + \alpha)A_{ij} + (\beta - \omega^2)B_{ij} + \gamma C_{ij} + \delta D_{ij} \tag{2.39}$$

and the propagator becomes:

$$\Delta(K) = \Delta_A \mathbf{A} + (k^2 - \omega^2 + \alpha + \gamma)\Delta_G \mathbf{B} + [(\beta - \omega^2)\Delta_G - \Delta_A]\mathbf{C} - \delta\Delta_G \mathbf{D} \tag{2.40}$$

with

$$\Delta_A^{-1}(K) = k^2 - \omega^2 + \alpha, \tag{2.41}$$

$$\Delta_G^{-1}(K) = (k^2 - \omega^2 + \alpha + \gamma)(\beta - \omega^2) - k^2\tilde{n}^2\delta^2 \tag{2.42}$$

These two equations give the dispersion relations for the gluonic modes in an anisotropic quark-gluon plasma.

In anisotropic plasma, the spacelike component of the self-energy tensor (in Eq.2.17) can be written as [71]

$$\Pi_p^{ij}(K) = -g^2 \int \frac{d^3p}{(2\pi)^3} v^i \partial^l f(\mathbf{p}) \Big(\delta^{jl} + \frac{v^j k^l}{K.V + i\epsilon}\Big) \tag{2.43}$$

where $f(\mathbf{p})$ is anisotropic distribution function. Using Eq.(2.34), one can simplify Eq.(2.43) to

$$\Pi^{ij}(K) = m_D^2 \sqrt{1+\xi} \int \frac{d\Omega}{(4\pi)} v^i \frac{v^l + \xi(\mathbf{v}.\hat{\mathbf{n}})n^l}{(1+\xi(\mathbf{v}.\hat{\mathbf{n}})^2)^2} \Big(\delta^{jl} + \frac{v^j k^l}{K.V + i\epsilon}\Big) \tag{2.44}$$

where m_D is the Debye mass, represented by

$$m_D^2 = -\frac{g^2}{2\pi^2} \int_0^\infty dp p^2 \frac{df_{\rm iso}(p^2)}{dp}. \tag{2.45}$$

Stable Mode

First, we discuss the stable collective modes which have poles at real-valued $\omega > |\mathbf{k}|$. Δ_G^{-1} can be factorized to obtain

$$\Delta_G^{-1} = (\omega^2 - \Omega_+^2)(\omega^2 - \Omega_-^2), \tag{2.46}$$

where

$$\begin{aligned} \Omega_\pm^2 &= \frac{1}{2}[\Omega^2 \pm \sqrt{\Omega^4 - 4[(\alpha+\gamma+k^2)\beta - k^2\tilde{n}^2\delta^2]}] \\ &= \frac{1}{2}[\Omega^2 \pm \sqrt{(\alpha-\beta+\gamma+k^2)^2 + 4k^2\tilde{n}^2\delta^2}] \end{aligned} \tag{2.47}$$

and

$$\Omega^2 = \alpha + \beta + \gamma + k^2 \tag{2.48}$$

The square root in equation (2.47) is always positive for real $\omega > k$. This leads to at most two stable modes coming from Δ_G. Another stable mode comes from the zero of Δ_A^{-1}.

All the collective modes can be compactly written as [71]

$$\omega_\pm^2 = \Omega_\pm^2(\omega_\pm), \tag{2.49}$$

$$\omega_\alpha^2 = k^2 + \alpha(\omega_\alpha). \tag{2.50}$$

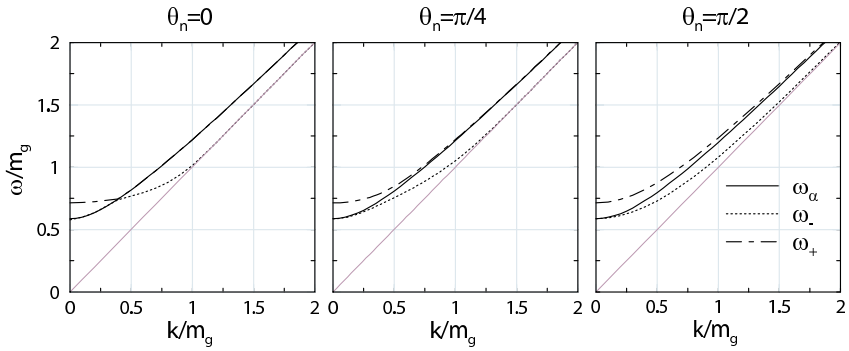

Figure 2.3: *Dispersion relation for the stable mode in anisotropic system. [71]*

For $\xi = 0$, $\omega_+ = \omega_\alpha = \omega_T$ and $\omega_- = \omega_L$. The resulting dispersion relations for all three modes for the case $\xi = 10$ and $\theta_n = \{0, \pi/4, \pi/2\}$ are shown in Fig. 2.3. We see that the stable modes depend on the angle of the propagation with respect to the anisotropy direction. It is clearly seen that all the three modes are shifted toward the light cone when the wave vector is orthogonal to the anisotropy direction.

Unstable Mode

In an anisotropic quark-gluon plasma, the propagator also has poles along the imaginary axis which indicates that the system possesses a magnetic instability [72, 102]. This can be identified as the so called filamentation or Weibel instability [103]. The instability is driven by the energy transferred from the particles to the field, which leads to a more rapid thermalization and equilibration of QGP.

For the unstable modes of the system we can write $\omega \to i\Gamma$ with Γ real valued and the solutions are written as

$$\begin{aligned} \Delta_G^{-1} &= (\Gamma^2 + \Omega_+)(\Gamma^2 + \Omega_-) = 0, \\ \Delta_A^{-1} &= \Gamma^2 + k^2 + \alpha = 0 \end{aligned} \tag{2.51}$$

where $\Omega_\pm$ are evaluated at $\omega = i\Gamma$. However, in contrast to the stable modes there is at most one solution in this case since numerically we find that $\Omega_+^2 > 0$ for all $\Gamma > 0$. For

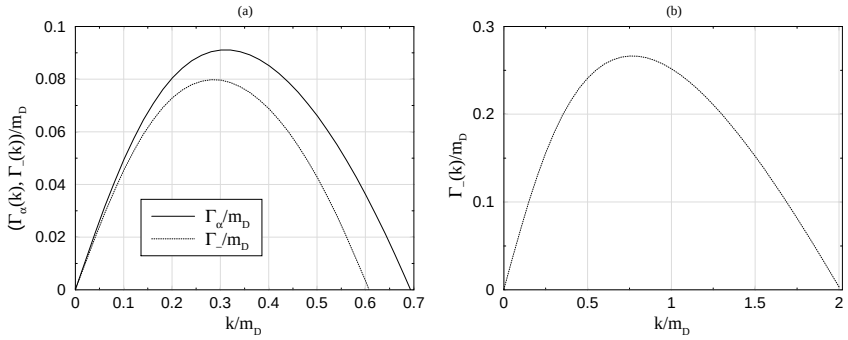

Figure 2.4: *Dispersion relation for the unstable mode in anisotropic system with (a)* $\xi = 10$*,* $\theta_n = \pi/8$ *and (b)* $\xi = 0.9, \theta_n = \pi/2$*.*

$\xi > 0$ there are two unstable modes in the system which can be found by solving

$$\Gamma_-^2 = -\Omega_-^2(i\Gamma_-), \tag{2.52}$$

$$\Gamma_\alpha^2 = -k^2 - \alpha(i\Gamma_\alpha) \tag{2.53}$$

We found that for $\xi > 0$, there were two unstable modes shown in Fig. 2.4(a), whereas $\xi < 0$, we find one unstable collective mode coming from Γ_-. Fig. 2.4(b) shows the unstable mode $\Gamma_-(k)$ with $\xi = -0.9$ and $\theta_n = \pi/2$.

• ○ •

Chapter 5

Probes of Anisotropy Quark-Gluon Plasma

As discussed earlier, there are various indirect probes to identify QGP which is usually assumed to be isotropic. However, to characterize the anisotropic QGP we have to look for signals which are sensitive to the momentum distribution (anisotropic) of the plasma particles. The effect of pre-equilibrium momentum anisotropy on various observables have been studied quite extensively over the past few years. For examples, electromagnetic probes (photons, dileptons) [99, 100, 131, 134, 135, 136, 137, 138, 139, 140], nuclear modification factor $vis-a-vis$ energy loss [132, 141, 142, 143, 144], gluon dissociation of J/ψ [33, 145] etc. have been suggested for the characterization of the AQGP. In Refs. [99] the direct photon yield has been calculated and contrasted with the RHIC data. For the fixed initial condition, the pre-equilibrium momentum anisotropy enhances high-energy photon by an order of magnitude [100]. Similar observations has been reported for the dilepton rate [134]. The authors of Ref. [134] have shown that the isotropization time $\tau_{\rm iso}$ can be extracted by comparing with the experimental data. It is found that the extracted value of $\tau_{\rm iso}$ lies within $1 < \tau_{\rm iso} < 1.5$ fm/c. In case of heavy quark, energy loss and momentum broadening in anisotropic QGP have also been investigated [146, 147, 148].

Another important observables to characterize the anisotropic plasma is the two-particle correlation. Size of the system during freeze-out is determined by two hadron correla-

tion [149]. We devoted our analysis for the full evolution of the fireball to observe the anisotropic effect on the size of the emission zone. Such analysis helps in understanding the effect of the anisotropy on the space-time dynamics of the evolving source.

However, photons and dileptons have the advantages of determining the dimension of the collision zone from very beginning as these probes leaves the plasma as soon as they are produced.

In the following section we briefly discuss the space-time evaluation of the matter in AQGP. In section 5.2, we investigate the impact of the early momentum space anisotropy on the nuclear modification factor of light hardons. In section 5.3, we calculate the gluon dissociation cross section of J/ψ in an anisotropic QGP. We extended our studies on two photon correlation coming from the isotropic and anisotropic QGP in section 5.4. The conclusions of this chapter are presented in section 5.5.

5.1 Space-time evaluation

For a dynamically evolving plasma the anisotropy parameter ξ and the hard momentum scale $p_{\rm hard}$ are time dependent. To construct this, two new parameter has been introduced: (1) $\tau_{\rm iso}$ which is the proper time at which the system begins behaving hydro-dynamically and (2) γ, which sets the sharpness of the transition from the early-time pre-equilibrium dynamics to late -time equilibrated dynamics. There are three possible scenarios of the space-time evaluation which are likely: (i) $\tau_{\rm iso} = \tau_i$, the system evolves hydro-dynamically so that $\xi = 0$ and $p_{\rm hard}$ can be identified with the temperature (T) of the system (ii) $\tau_{\rm iso} \to \infty$, the system never comes to equilibrium, (iii) $\tau_{\rm iso} > \tau_i$ and $\tau_{\rm iso}$ is finite, one should devise a time evolution model for ξ and $p_{\rm hard}$ which smoothly interpolates between pre-equilibrium anisotropy and hydrodynamics. This model can be executed mathematically by generalizing the anisotropic parameter $\xi(\tau)$ as follows;

$$\xi(\tau) = \left(\frac{\tau}{\tau_i}\right)^{\delta} - 1. \tag{5.1}$$

The limit $\delta = 0$ correspond to scenario (i) where expansion is hydrodynamical . On the other hand, the limits $\delta \neq 0$ and $\xi \neq 0$ correspond to scenario (ii) where the system is highly anisotropic. For the present work we shall be following scenario (iii) which interpolates between hydrodynamic evolution and the anisotropic evolution. The time dependences of various parameters are obtained in terms of a smeared step function as follows[67, 131]:

$$\Lambda(\tau, \tau_{\rm iso}, \gamma) = \frac{1}{2}(\tanh[\gamma(\tau - \tau_{\rm iso})/\tau_{\rm iso}] + 1). \tag{5.2}$$

It is clear from the above equation that for $\tau \ll \tau_{iso}$, $\lambda \to 0$ (anisotropic evolution) and for $\tau \gg \tau_{iso}$, $\lambda \to 1$ (hydrodynamic evolution).Thus, the time dependences of ξ and $p_{\rm hard}$ are as follows [131, 143]:

$$\begin{aligned} \xi(\tau) &= a^{\delta[1-\lambda(\tau)]} - 1, \\ p_{\rm hard}(\tau) &= T_i \, [\mathcal{U}(\tau)/\mathcal{U}(\tau_i)]^{1/3}, \end{aligned} \tag{5.3}$$

where

$$\begin{aligned} \mathcal{U}(\tau) &\equiv \left[\mathcal{R}\left(a_{iso}^{\delta} - 1\right)\right]^{3\lambda(\tau)/4} (a_{iso}/a)^{1-\delta[1-\lambda(\tau)]/2}, \\ \mathcal{R}(x) &\equiv \frac{1}{2}\left[\frac{1}{1+x} + \frac{\arctan\sqrt{x}}{\sqrt{x}}\right], \end{aligned} \tag{5.4}$$

with $a \equiv \tau/\tau_i$ and $a_{iso} \equiv \tau_{iso}/\tau_i$. The power of $\mathcal{R}$ in $\mathcal{U}$ keeps energy density continuous at $\tau = \tau_{iso}$ for all γ. For isotropic case, we have $p_{\rm hard} = T$, $\tau_{\rm iso} = \tau_i$ so that $\Lambda = 1, \mathcal{U}(\tau) = \tau_i/\tau$, and $\mathcal{U}(\tau_i) = 1$. By using $c_s^2 = 1/3$ we recover the Bjorken cooling law [19]. In the present work it is assumed that an isotropic QGP is formed at an initial temperature T_i and initial time τ_i. In case of isotropic expansion the experimentally measured hadron multiplicity can be related to the initial temperature and thermalization time by the following equation [43]:

$$T_i^3(b_m)\tau_i = \frac{2\pi^4}{180\zeta(3)\pi\, R_T^2 a_k}\left\langle \frac{dN}{dy}(b_m)\right\rangle \tag{5.5}$$

where $\left\langle dN/dy(b_m)\right\rangle$ is the hadron (predominantly pions) multiplicity for a given centrality class with maximum impact parameter b_m. R_T is the transverse dimension of the system, τ_i is the formation time, $\zeta(3)$ is the Riemann zeta function.

The parton energy density in an anisotropic plasma can be factorized in the following manner:

$$\mathcal{E}(\tau) \;=\; \mathcal{E}_0\,[\mathcal{U}(\tau)/\mathcal{U}(\tau_i)]^{4/3}, \tag{5.6}$$

where $\mathcal{E}_0$ is the parton energy density in an isotropic plasma.

In the following section we assume that the plasma expands longitudinally and the effect of transverse expansion at the early stage might be neglected [150]. Since the momentum space anisotropy is an early stage phenomenon, this assumption is justified. Even if the transverse expansion is important in the very early stage, it will have two effects so far as the parton energy loss is concerned : (i) The expanding geometry will increase the duration of propagation, and (ii) the same expansion will cause the parton density to fall along its path. These two effects partially compensate each other and the energy loss is almost the same as in the case without the transverse expansion [151]. As the colliding nuclei do have a transverse density profile, we assume that the initial temperature profile is given by [152]

$$T_i(r) = T_i\,\left[2\left(1 - r^2/R_T^2\right)\right]^{1/4}. \tag{5.7}$$

Using Eqs. (5.3) and (5.7) we obtain the profile of the hard momentum scale as

$$p_{\rm hard}(\tau, r) = T_i\,\left[2\left(1 - r^2/R_T^2\right)\right]^{1/4}[\mathcal{U}(\tau)/\mathcal{U}(\tau_i)]^{1/3}. \tag{5.8}$$

5.2 Nuclear modification factor in an anisotropic quark-gluon plasma

It is well-known that the energy loss of the partons in QCD plasma can proceed in two ways, namely collisional process and radiative process via gluon radiation. At the early stage of momentum anisotropy, any calculation of energy loss should, in principle, include this aspect. The collisional energy loss for heavy fermion has been calculated in anisotropic media in Ref. [153, 26] and it is found that the deviations from the isotropic result are of the order of 10% for $\xi = 1.$ and it also increases with the increase of anisotropy parameter

ξ. Radiative energy loss in anisotropic QGP has been calculated in Ref. [143] in the first order opacity expansion where the scatterers are static. It is observed that the energy loss of a parton in an anisotropic media depends both on the anisotropy parameter and the direction of propagation with respect to the anisotropy axis. In this section we calculate the fractional energy loss due to the gluon radiation in an infinite size anisotropic media treating the scatters as providing a screened Coulomb-like potential. The results will then be applied to calculate hadronic p_T-spectrum and nuclear modification factor ($\mathrm{R_{AA}}$).

5.2.1 Radiative energy loss

We consider scatterings from static charge in which case only longitudinal gauge bosons are exchanged. Contribution of the Feynman diagrams to the soft-gluon radiation in a static medium at first order in opacity is shown in Fig. 5.1. We also assume that an on-

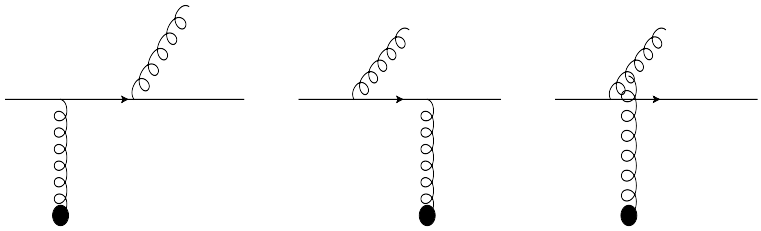

Figure 5.1: Feynman diagrams contributing to the soft gluon radiation in a static medium to first order in opacity.

shell quark produced in the remote past is propagating through an infinite QCD medium that consists of randomly distributed static scattering centers [154]. In the Gyulassy-Wang formalism [155] static interaction is modeled using a color-screened Yukawa potential originally developed for the isotropic QCD medium and is given by

$$\begin{aligned} V_n &= V(q_n)\exp[i\vec{q}_n.\vec{x}_n] \\ &= 2\pi\delta(q^0)\frac{4\pi\alpha_s}{(\vec{q}_n^2+m_D^2)}\exp[i\vec{q}_n.\vec{x}_n]T_{a_n}(R)\otimes T_{a_n}(n), \end{aligned} \tag{5.9}$$

The quantity x_n is the location of the nth scattering center, T (summed over a_n) denotes the colour matrices of the parton and the scattering center. It is to be noted that the potential has been derived by Hard Thermal Loop (HTL) perturbation theory. The momentum space anisotropy affects the two-body interaction and it becomes direction dependent. The radiative energy loss, will also depend on the direction of momentum of the quarks emitting Bremsstrahlung gluons. This necessitates the introduction of anisotropy dependent potential to estimate the radiative energy loss in a plasma having anisotropic momentum distribution. To calculate the heavy-quark potential in anisotropic medium one starts with the retarded gluon self-energy expressed as [80]

$$\Pi^{\mu\nu}(P) = g^2 \int \frac{d^3k}{(2\pi)^3} v^\mu \frac{\partial f(\vec{k})}{\partial K^\beta} \left(g^{\nu\beta} - \frac{v^\nu P^\beta}{P\cdot v + i\epsilon} \right) \tag{5.10}$$

We have adopted the following notation for four vectors: $P^\mu = (p_0, \vec{p}) = (p_0, \mathbf{p}, p_z)$, i. e. $\vec{p}$ describes a three-vector while $\mathbf{p}$ denotes the two-vector transverse to the z-direction.

With the structure function in Eqs.(2.36) we can construct the effective gluon propagator in an anisotropic media and it can be expressed as [156, 157]:

$$\begin{aligned} \Delta^{\mu\nu} &= \frac{1}{(P^2-\alpha)}[A^{\mu\nu} - C^{\mu\nu}] \\ &+ \Delta_G\Big[(P^2-\alpha-\gamma)\frac{\omega^4}{P^4}B^{\mu\nu} + (\omega^2-\beta)C^{\mu\nu} + \delta\frac{\omega^2}{P^2}D^{\mu\nu}\Big] - \frac{\lambda}{P^4}P^\mu P^\nu, \end{aligned} \tag{5.11}$$

where

$$\Delta_G^{-1} = (P^2-\alpha-\gamma)(\omega^2-\beta) - \delta^2[P^2-(n\cdot P)^2]. \tag{5.12}$$

Now we can easily calculate the anisotropy dependent momentum space potential. It can be obtained from the static gluon propagator in the following way [143]:

$$\begin{aligned} v(\mathbf{q}, q_z, \xi) &= g^2\,\Delta^{00}(\omega=0, \mathbf{q}, q_z, \xi) \\ &= g^2\,\frac{\vec{q}^2 + m_\alpha^2 + m_\gamma^2}{(\vec{q}^2 + m_\alpha^2 + m_\gamma^2)(\vec{q}^2 + m_\beta^2) - m_\delta^2}, \end{aligned} \tag{5.13}$$

where the expression for $m_\alpha^2, m_\beta^2, m_\gamma^2$ and m_δ^2 are given in the Appendix B. For $q_z = 0$, the two-body potential in an anisotropic medium simplifies to

$$v(\mathbf{q},\xi) = \frac{4\pi\alpha_s}{\mathbf{q}^2 + R(\xi)m_D^2}, \tag{5.14}$$

with

$$R(\xi) = \frac{1}{2}\Big[\frac{1}{1+\xi} + \frac{\tan^{-1}\sqrt{\xi}}{\sqrt{\xi}}\Big] \tag{5.15}$$

and m_D is given by $m_D^2 = g^2\, p_{\rm hard}^2\,(1 + N_F/6)$, where N_F is the number of flavors.

Now the parton scatters with one of the colour center with the momentum $Q = (0, \mathbf{q}, q_z)$ and subsequently radiates a gluon with momentum $K = (\omega, \mathbf{k}, k_z)$. The quark energy loss is calculated by folding the rate of gluon radiation ($\Gamma(E)$) with the gluon energy by assuming $\omega + q_0 \approx \omega$. In the soft scattering approximation one finds the quark radiative energy loss per unit length as [154],

$$\frac{dE}{dL} \;=\; \frac{E}{D_R}\int x\frac{d\Gamma}{dx}dx \tag{5.16}$$

Here D_R is defined as $[t_a, t_c][t_c, t_a] = C_2(G)C_R D_R$, where $C_2(G) = 3$, $D_R = 3$ and $[t_a, t_c]$ is a color commutator. x is the longitudinal momentum fraction of the quark carried away by the emitted gluon. Now in anisotropic media we find [143],

$$x\frac{d\Gamma}{dx} \;=\; \frac{C_R\alpha_s}{\pi}\frac{L}{\lambda}\int\frac{d^2\mathbf{k}}{\pi}\frac{d^2\mathbf{q}}{\pi}|v(\mathbf{q},\xi)|^2\frac{m_D^2}{16\pi^2\alpha_s^2}\left[\frac{\mathbf{k}+\mathbf{q}}{(\mathbf{k}+\mathbf{q})^2+\chi^2} - \frac{\mathbf{k}}{\mathbf{k}^2+\chi}\right]^2, \tag{5.17}$$

where $\chi == m_q^2x^2 + m_g^2$ with $m_g^2 = m_D^2/2$ and $m_q^2 = m_D^2/6$. λ denotes the average mean free path of the quark given by

$$\frac{1}{\lambda} = \frac{1}{\lambda_g} + \frac{1}{\lambda_q}, \tag{5.18}$$

which depends on the strength of the anisotropy. It is to be noted that λ_g and λ_q correspond to the contributions to the mean free path of the propagating quark coming from q-g and q-q scatterings, respectively. The mean free path can be expressed with the help of Eq.(5.14) and we have

$$\lambda_i^{-1} = \frac{C_R C_2(i)\rho(i)}{N_c^2 - 1}\int\frac{d^2\mathbf{q}}{(2\pi)^2}|v(\mathbf{q},\xi)|^2, \tag{5.19}$$

where $C_R = 4/3$, $C_2(i)$ is the Casimir for d_i-dimensional representation and $C_2(i) = (N_c^2 - 1)/(2N_c)$ for quark and $C_2(i) = N_c$ for gluon scatterers and ρ_i is the density of the scatterers. Using $\rho_i = \rho_i^{\rm iso}/\sqrt{1+\xi}$ we obtain

$$\frac{1}{\lambda} = \frac{18\alpha_s p_{\rm hard}\zeta(3)}{\pi^2\sqrt{1+\xi}}\frac{1}{R(\xi)}\frac{1+N_F/6}{1+N_F/4}. \tag{5.20}$$

In the present scenario, we assume that the parton is propagating along the z direction and makes an angle θ_n with the anisotropy direction. In such case, we replace $\mathbf{q}$ and q_z in Eq.(5.13) by $\mathbf{q} \to \sqrt{\mathbf{q}^2 - \mathbf{q}^2\sin^2\theta_n\cos^2\phi}$ and $q_z \to |\mathbf{q}|\cos\phi\sin\theta_n$, where $\mathbf{q} = (|\mathbf{q}|\cos\phi, |\mathbf{q}|\sin\phi)$. For arbitrary ξ the radiative energy loss can be written as [143, 144]

$$\begin{aligned}\frac{\Delta E}{E} &= \frac{C_R\alpha_s}{\pi^2}\frac{L}{\lambda}\int dx d^2\mathbf{q}|\frac{m_D^2}{(\mathbf{q}^2+R(\xi)m_D^2)^2}\Bigg[-\frac{1}{2}-\frac{k_m^2}{k_m^2+\chi}\\ &+ \frac{\mathbf{q}^2-k_m^2+\chi}{2\sqrt{\mathbf{q}^4+2\mathbf{q}^2(\chi-k_m^2)}+(k_m^2+\chi)^2}+\frac{\mathbf{q}^2+2\chi}{\mathbf{q}^2\sqrt{1+\frac{4\chi}{\mathbf{q}^2}}}\\ &\times \ln\left(\frac{[k_m^2/\chi+1](\mathbf{q}^2+3\chi)+\sqrt{1+\frac{4\chi}{\mathbf{q}^2}}(\mathbf{q}^2+\chi)}{(\mathbf{q}^2-k_m^2+3\chi)+\sqrt{1+\frac{4\chi}{\mathbf{q}^2}}\sqrt{\mathbf{q}^4+2\mathbf{q}^2(\chi-k_m^2)}+(k_m^2+\chi)^2}\right)\Bigg]. \end{aligned}\tag{5.21}$$

The fractional energy loss in anisotropy medium for the light quark is shown in Fig. 5.2. We consider a plasma at a temperature $T = 200$ MeV with the effective number of degrees of freedom $N_F = 2.5$ The value of the strong coupling constant is taken as $\alpha_s = 0.3$ and the length of the medium is $L = 5$ fm. The energy loss in the anisotropic medium depends on the angle of propagation of the fast parton with respect to the anisotropy axis [143]. It is clearly seen that as the anisotropic parameter increases, the fractional energy loss increases when the quark propagates along the direction of anisotropy. It is observed that at low momentum the enhancement is more and after that it almost saturates for all the values of ξ considered here. The enhancement factor can be better understood by looking at the right panel of Fig. 5.2 where we have plotted the ratio of the fractional energy loss in anisotropic media to that in isotropic case. For large value of ξ, the ratio is seen to increase reaching a maximum value of the order of 1.5 corresponding to $\xi = 5$. This is because the energy loss is proportional to the square of the two-body potential $v(\mathbf{q}, \xi)$ which increases with ξ and hence the fractional energy loss increases with ξ.

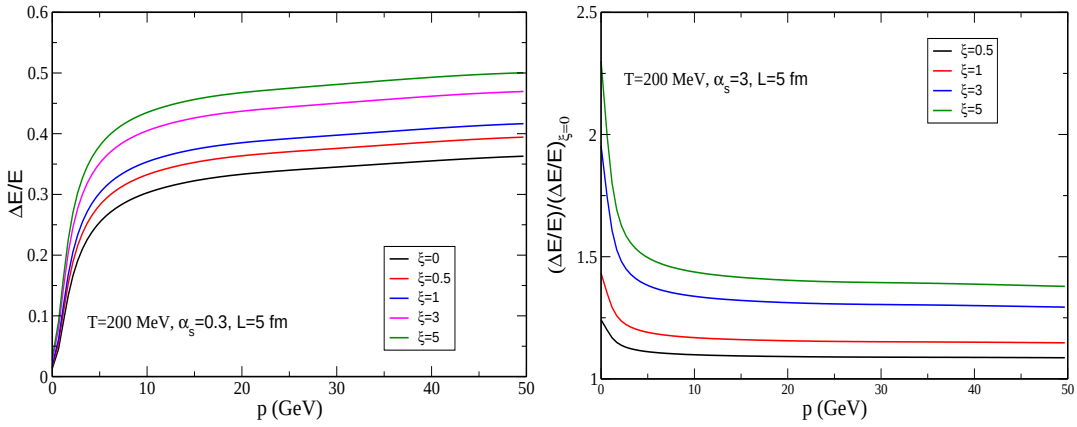

Figure 5.2: Fractional energy loss for light quark for $\xi = (0, 0.5, 1, 3, 5)$ (left panel). The ratio of the fractional energy loss of anisotropic media to that in isotropic media is also presented (right panel).

5.2.2 Hadronic p_T spectrum

Now we calculate the nuclear modification factor of light hadrons incorporating the light quark energy loss in AQGP. Starting with two-body scattering at the parton level, the differential cross-section for the jet production can be calculated using the following relation [158]:

$$E\frac{d\sigma}{d^3p}(AB \to \text{jet} + X) = K \sum_{abcd} \int dx_a dx_b G_{a/h_A}(x_a, Q^2)\, G_{b/h_B}(x_b, Q^2) \times \frac{\hat{s}}{\pi}\frac{d\sigma}{d\hat{t}}(ab \to cd)\delta(\hat{s} + \hat{t} + \hat{u}), \tag{5.22}$$

where the factor K is introduced to take into account the higher-order effects and $G_{a/h_A}(G_{b/h_B})$ is the parton distribution function (PDF) of the incoming parton $a(b)$ in the incident hadron $A(B)$, which depends on the momentum fraction $x_a(x_b)$. The argument of the δ function can be expressed in terms of x_a and x_b and doing the x_b integration we arrive at the final expression given by,

$$E\frac{d\sigma}{d^3p}(AB \to \text{jet} + X) = K \sum_{abcd} \int_{x_{\text{amin}}}^{1} dx_a G_{a/h_A}(x_a, Q^2)\, G_{b/h_B}(x_b, Q^2)$$

$$\times \quad \frac{2}{\pi}\frac{x_a x_b}{2x_a - x_T e^y}\frac{d\sigma}{d\hat{t}}(ab \to cd), \tag{5.23}$$

where $x_b = (x_a x_T e^{-y})/(2x_a - x_T e^y)$, $x_T = 2p_T/\sqrt{s}$ and $x_{\rm amin} = (x_T e^y)/(2 - x_T e^{-y})$. It should be noted that to obtain single particle inclusive invariant cross-section for hadron production in hadron-hadron collisions, the fragmentation function $D_{h/c}(z, Q^2)$ must be introduced. To obtain the hadronic p_T spectra in A-A collisions, we multiply the result by the nuclear overlap function for a given centrality. However, the inclusion of jet-quenching as a final state effect in nucleus-nucleus collisions, can be implemented in two ways: (i) modifying the fragmentation function [159] and (ii) modifying the partonic p_T spectra [160] but keeping the fragmentation function unchanged. In this calculation we intend to modify the fragmentation function. The effective fragmentation function can be written as

$$D_{h/c}(z, Q^2) = \frac{z^*}{z} D_{h/c}(z^*, Q^2) \tag{5.24}$$

where, $z^* = z/(1 - \Delta E/E)$ is the modified momentum fraction. We use the energy loss expression given by Eq.(5.21) which is derived to first order in opacity. Now we take into account the jet production geometry. We assume that all the jets are not produced at the same point and the path length traversed by these partons before fragmentation are not the same. We consider a jet initially produced at (r, ϕ) leaves the plasma after a proper time or equivalently after traversing a distance L where

$$L(r, \phi) = \sqrt{R_T^2 - r^2 \sin\phi^2} - R_T \cos\phi, \tag{5.25}$$

where R_T is the transverse dimension of the system. Now the hadron p_T spectra depends on the path length the initial parton must travel and the temperature profile along that path. Since the number of jets produced at $\vec{r}$ is proportional to the number of binary collisions, the probability is proportional to the product of thickness functions:

$$\mathcal{P}(\vec{r}) \propto T_A(\vec{r})\, T_B(\vec{r}) \tag{5.26}$$

For a hard sphere $\mathcal{P}(r)$ is given by

$$\mathcal{P}(r) = \frac{2}{\pi R_T^2}\left(1 - \frac{r^2}{R_T^2}\right)\theta(R_T - r) \tag{5.27}$$

where $\int d^2r\,\mathcal{P}(r) = 1$. To obtain the hadron p_T spectra, we have to convolute the resulting expression over all the transverse positions and it becomes

$$\begin{aligned}\frac{dN^{\pi^0(\eta)}}{d^2p_T dy} &= \sum_f \int d^2r\mathcal{P}(r) \int_{t_i}^{t_L} \frac{dt}{t_L - t_i} \int \frac{dz}{z^2} \\ &\quad \times D_{\pi^0(\eta)/f}(z, Q^2)|_{z=p_T/p_T^f}\, E\frac{dN}{d^3p^f},\end{aligned} \tag{5.28}$$

Here, the initial momentum distribution of jets is $E\frac{dN}{d^3p^f}$ and can be computed using LO-pQCD as mentioned earlier. The average value of distance traversed by the partons, $\langle L\rangle$ can be calculated as

$$\langle L\rangle = \frac{\int_0^{R_T} rdr \int_0^{2\pi} L(\phi, r)T_{AA}(r, b=0)d\phi}{\int_0^{R_T} rdr \int_0^{2\pi} T_{AA}(r, b=0)d\phi}, \tag{5.29}$$

where $\langle L\rangle \sim 5.8(6.2)fm$ for RHIC (LHC). Finally, the nuclear modification factor, R_{AA} is defined as

$$R_{AA}(p_T) = \frac{\frac{dN_{AA}^{\pi^0(\eta)}}{d^2p_T dy}}{\left[\frac{dN_{AA}^{\pi^0(\eta)}}{d^2p_T dy}\right]_0} \tag{5.30}$$

where $\left[\frac{dN_{AA}^{\pi^0(\eta)}}{d^2p_T dy}\right]_0$ corresponds to the hadron p_T distribution without energy loss.

In the present work, we have used a free streaming interpolating model that interpolates between early-time longitudinal free streaming and late-time ideal hydrodynamic expansion by choosing $\delta = 2$. we use two sets of initial condition for RHIC energies. The initial condition are taken as $T_i = 440$MeV ($T_i = 350$MeV) and $\tau_i = 0.147$ fm/c ($\tau_i = 0.24$ fm/c) in the left (right) panel of Fig. 5.3 which describes the nuclear modification factor for various values of isotropization time, $\tau_{\rm iso}$ along with the PHENIX data [161]. It is observed that as $\tau_{\rm iso}$ increases, the value of $R_{\rm AA}$ decreases compared to its isotropic value. This is because the hard scale $p_{\rm hard}$ decreases slowly as compared to the isotropic case, i.e. the cooling is slow. For reasonable choices of $\tau_{\rm iso}$, the experimental data is well described. It is quite clear from left panel of Fig. 5.3 that the extracted value of isotropization time lies in

the range $0.5 \leq \tau_{\rm iso} \leq 1.5$ fm/c. This is in agreement with the earlier finding of $\tau_{\rm iso}$ using PHENIX photon data [100]. In the right panel of Fig. 5.3 we observe that to reproduce the data, larger value of $\tau_{\rm iso}$ is needed as compared to the case of higher initial temperature. We extract an upper limit of $\tau_{\rm iso} = 2$ fm/c in this case. Further increase of $\tau_{\rm iso}$ leads to more suppression thereby under-predicting the data. However, unlike the RHIC data, our present model is unable to explain the LHC data [144].

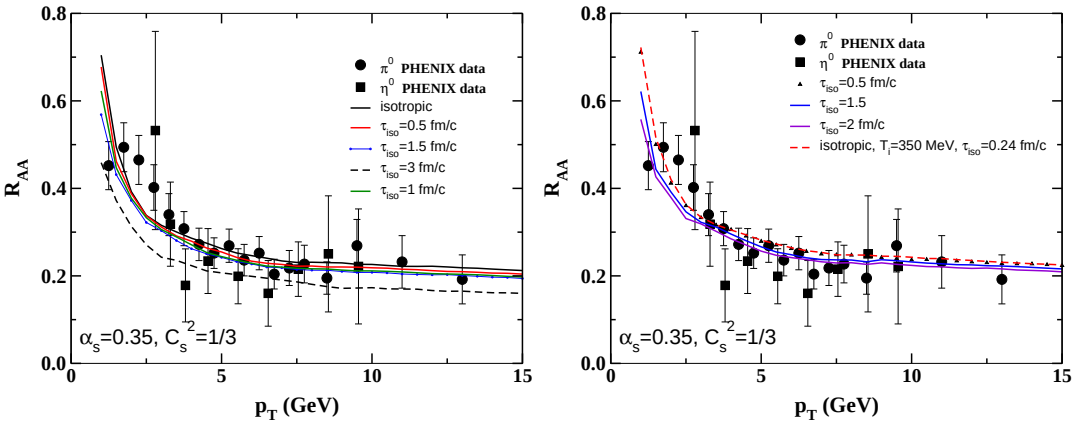

Figure 5.3: Nuclear modification factor at RHIC energies. The initial condition are taken as $T_i = 440$MeV ($T_i = 350$MeV) and $\tau_i = 0.147$ fm/c ($\tau_i = 0.24$ fm/c) in the left (right) panel.

So far we have used the interpolating model which assumes fixed initial conditions. But, most of the experimental results correspond to fixed final multiplicity (FFM). Thus, we should device a mechanism which enforces FFM. To do this the initial condition will have to be varied as a function of assumed isotropization time, i.e., one must lower the initial "temperature" for finite $\tau_{\rm iso}$. To accomplish this model one has to redefine $\mathcal{U}(\tau)/\mathcal{U}(\tau_i)$ in Eq.(5.3) as [134]:

$$\mathcal{U}(\tau)/\mathcal{U}(\tau_i) = \mathcal{U}(\tau)\left[\mathcal{R}((\tau_{iso}/\tau_i)^{\delta} - 1)\right]^{-3/4}(\tau_i/\tau_{iso}) \tag{5.31}$$

As a consequence of this modification the initial "temperature" will depend on the assumed value of $\tau_{\rm iso}$.

The result for the FFM condition at RHIC energies has been displayed in Fig. 5.4. In this case the value of $R_{\rm AA}$ increases with $\tau_{\rm iso}$ compared to the isotropic case. The reason for this is that in FFM the larger the value of $\tau_{\rm iso}$ is, the lower is the initial hard momentum scale resulting less energy loss. This gives rise to higher value of $R_{\rm AA}$ as compared to the fixed initial condition case as well as the isotropic case. It is also seen that for FFM isotropic value of the nuclear modification factor is closer to the data. Thus, it is quite clear that the use of FFM does not lead to any firm conclusion about the extraction of $\tau_{\rm iso}$.

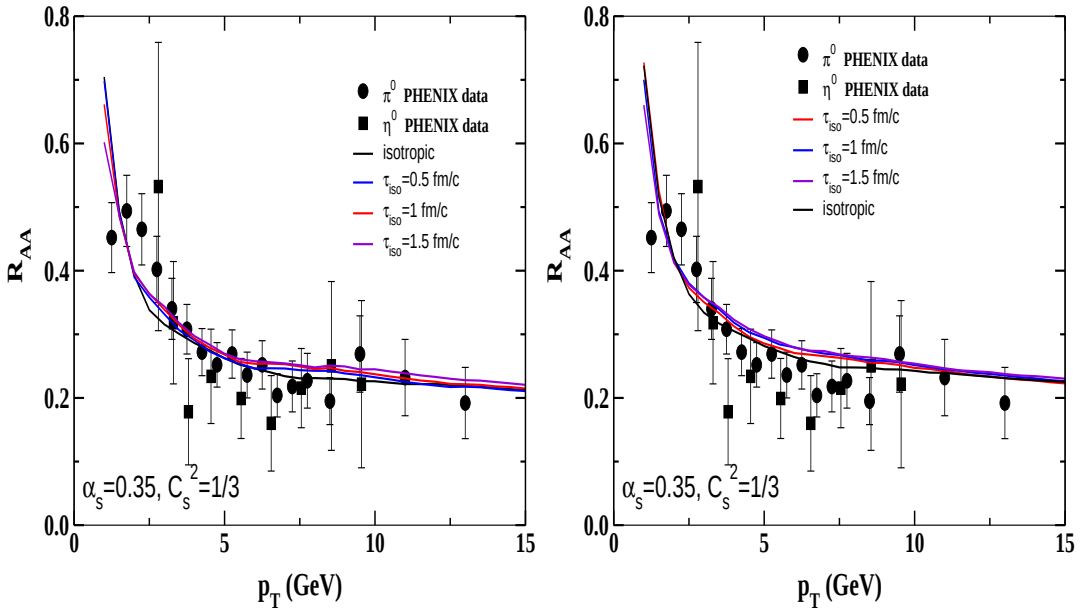

Figure 5.4: Same as Fig. 5.3 for fixed final multiplicity.

5.3 Gluon dissociation of J/ψ in an anisotropic quark-gluon plasma

Charm quark can be produced during the early stages of heavy-ion collisions, when partonic degrees of freedom are relevant. The production of charm quark bound state (J/ψ mesons)

is suppressed due to color screening [32]. J/ψ suppression can be used to obtain the convincing evidence of the existence of the QGP in heavy-ion collisions. The interaction of J/ψ with deconfined partons and hadrons are different. In a QGP the much harder gluons can easily break up a J/ψ contrary to the case of hadronic system. The dissociation of J/ψ will continue during the whole equilibration process until the beginning of hadronization or effective temperature drops below a certain value.

In the following we will discuss the effect of the initial state momentum anisotropy on the survival probability of J/ψ due to the gluon dissociation.

5.3.1 The thermal-averaged Gluon-J/ψ dissociation cross section

Peskin and Bhanot first calculated the quarkonium-hadron interaction cross section using operator product expansion [162]. This formalism allows to express the hadron-J/ψ inelastic cross section in terms of the convolution of the inelastic gluon-J/ψ dissociation cross section with the gluon distribution inside the hadron. The gluon-J/ψ dissociation cross section is given by[163]

$$\sigma(q^0) = \frac{2\pi}{3}\left(\frac{32}{3}\right)^2\left(\frac{16\pi}{3g_s^2}\right)\frac{1}{m_Q^2}\frac{(q^0/\epsilon_0-1)^{3/2}}{(q^0/\epsilon_0)^5}\ , \tag{5.32}$$

where q^0 is the energy of the gluon in the stationary J/ψ frame and its value must be greater than the J/ψ binding energy ϵ_0. g_s is the coupling constant and m_Q is charm quark mass. The maximum value of the gluon J/ψ dissociation cross section [163] is about 3 mb in the range $0.7 \leq q^0 \leq 1.7$ GeV. Therefore low-momentum gluons do not have the resolution to distinguish the heavy constituent quarks or the energy to excite them to the continuum. On the other hand, the high-momentum gluons do not see the large object and simply passes through it. In the present work, we assume that the binding energy of J/ψ is constant in AQGP at finite temperature. However, using the real and imaginary part of heavy quark potential in Schrodinger equation the authors of Ref. [164] have shown that the binding energy of quarkonium states strongly depends on the anisotropy parameter as well as on the hard momentum scale.

We assume that the J/ψ moves with four-momentum P given by

$$P = (M_T \cosh y, 0, P_T, M_T \sinh y) \tag{5.33}$$

where $M_T = \sqrt{M_{J/\psi}^2 + P_T^2}$ is the J/ψ transverse mass and y is the rapidity of the J/ψ. A gluon with a four-momentum $K = (k^0, \mathbf{k})$ in the rest frame of the parton gas has energy $q^0 = K.u$ in the rest frame of the J/ψ. The thermal gluon-J/ψ dissociation cross section is defined as [33]

$$\langle \sigma(K.u) v_{\rm rel} \rangle_k = \frac{\int d^3k \sigma(K.u) v_{\rm rel} f(k^0, \xi, p_{\rm hard})}{\int d^3k f(k^0, \xi, p_{\rm hard})} \tag{5.34}$$

where $v_{\rm rel}$ is the relative velocity between the J/ψ and a gluon

$$v_{\rm rel} = \frac{P \cdot K}{E_{J/\psi} k^0} = 1 - \frac{\mathbf{k} \cdot \mathbf{P}}{k^0 M_T \cosh y}, \tag{5.35}$$

To calculate the velocity-averaged cross section in anisotropic media we note that the anisotropy enters through the distribution function [131, 145],

$$f(k^0, \xi, p_{\rm hard}) = \frac{1}{e^{k^0 \sqrt{1+\xi(\hat{k}.\hat{n})^2}/p_{\rm hard}} - 1}. \tag{5.36}$$

A change of variables ($K \leftrightarrow Q$) can be obtained by using Lorentz transformations:

$$\begin{aligned} k^0 &= \frac{1}{M_{J/\psi}} \Big[q^0 E + pq(\sin\theta_p \sin\theta_q \sin\phi_q + \cos\theta_p \cos\theta_q) \Big], \\ \mathbf{k} &= \mathbf{q} + \frac{qE}{|\mathbf{p}| M_{J\psi}} \Big[(M_T \cosh y - M_{J\psi})(\sin\theta_p \sin\theta_q \sin\phi_q + \cos\theta_p \cos\theta_q) + |\mathbf{p}| \mathbf{v}_{J/\psi} \Big], \end{aligned}$$

where $\mathbf{v_{J/\psi}} = \mathbf{p}/E$, $P = (E, 0, |\mathbf{p}| \sin\theta_p, |\mathbf{p}| \cos\theta_p)$ and $\mathbf{q} = (q \sin\theta_q \cos\phi_q, q \sin\theta_q \sin\phi_q, q \cos\theta_q)$ In the rest frame of J/ψ, the numerator of Eq.(5.34) can be written as

$$\int d^3q \frac{M_{J/\psi}}{E} \sigma(q^0) f(k^0, \xi, p_{hard}), \tag{5.37}$$

while the denominators of Eq.(5.34) can be written as [141]

$$\int d^3k f(k^0, \xi, p_{\rm hard}) = \frac{1}{\sqrt{1+\xi}} 8\pi\zeta(3) p_{\rm hard}^3, \tag{5.38}$$

where $\zeta(3)$ is the Riemann zeta function.

5.3.2 Survival probability of J/ψ in an anisotropic media

To calculate the survival probability of J/ψ in an anisotropic plasma, we will neglect the transverse expansion and consider only longitudinal expansion of the matter. A J/ψ produced at point $\mathbf{r}$ will travel a distance in the transverse direction with velocity $\mathbf{v}_{J/\psi}$ given by

$$d = -r\cos\phi + \sqrt{R_T^2 - r^2(1 - cos^2\phi)} \tag{5.39}$$

where $\cos\phi = \hat{v}_{J/\psi} \cdot \hat{r}$. The time interval $\tau_\psi = M_T d/P_T$ is the time before J/ψ escapes from a gluon gas of transverse extension R_T. With the thermal cross section, the survival probability of the J/ψ in the deconfined quark-gluon plasma is of the following form [33],

$$S(P_T) = \frac{\int d^2r(R_T^2 - r^2)\exp[-\int_{\tau_i}^{\tau_{\max}} d\tau n_g(\tau) < \sigma(K.u)v_{\rm rel} >_k]}{\int d^2r(R_T^2 - r^2)}, \tag{5.40}$$

where τ_i is the QGP formation time and $\tau_{\max} = min(\tau_\psi, \tau_c)$. In the case of anisotropic QGP τ_c is determined by the condition $p_{\rm hard}(\tau = \tau_c) = T_c$ [67], where $T_c \sim 170 - 200$ MeV. $n_g(\tau)$ is the gluon density at a given time τ. For an expanding plasma the anisotropy parameter ξ and the hard momentum scale $p_{\rm hard}$ are time dependent and governed by the Eqs.(5.3) and (5.8).

5.3.3 Results

Let us first discuss the numerical result of the thermally average gluon dissociation cross-section in the anisotropic system. In Fig. 5.5 we plot the thermally averaged gluon-J/ψ dissociation cross section as a function of $p_{\rm hard}$ at central rapidity region for $P_T = 0$ and $P_T = 8$ GeV for a set of values of the anisotropy parameter. It is seen that the cross section decreases with ξ for $p_{\rm hard}$ up to ~ 500 MeV and then increases as compared to the isotropic case ($\xi = 0$)(see in Fig. 5.5a). Similar feature has been observed in Fig. 5.5b for higher P_T where the cross section starts to increase beyond $p_{\rm hard} \sim 200$ MeV. The dissociation cross section depends on the direction of propagation (θ_p) of the quarkonium with respect to the

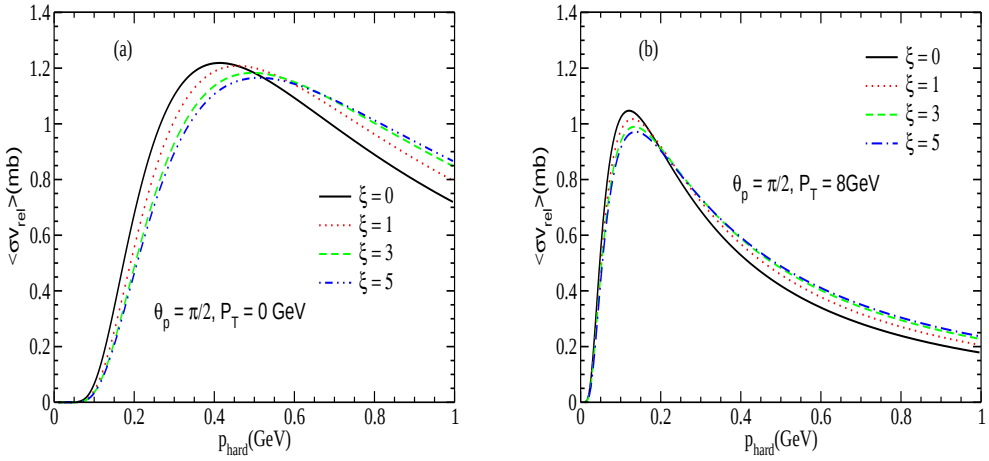

Figure 5.5: The thermal-averaged gluon-J/ψ dissociation cross section as function of the hard momentum scale at central rapidity ($\theta_p = \pi/2$) for $\xi = \{0, 1, 3, 5\}$. (a) corresponds to $P_T = 0$ and (b) is for $P_T = 8$ GeV.

anisotropy axis as shown in Fig. 5.6. These observations will have important consequences while calculating the survival probability of J/ψ.

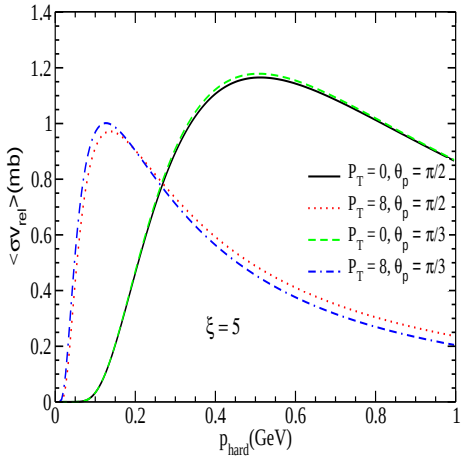

Figure 5.6: Direction dependence of thermal averaged gluon-J/ψ dissociation cross section for two values of P_T and at two different rapidities.

In Fig. 5.7 we display the dissociation cross section as a function of P_T of the J/ψ for

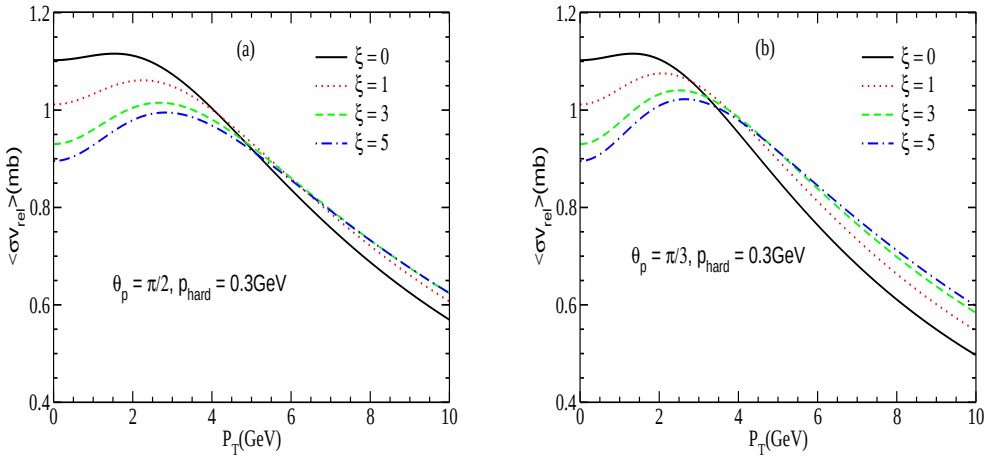

Figure 5.7: The thermal-averaged gluon-J/ψ dissociation cross section as a function of the transverse momentum P_T for $p_{\rm hard}$ at (a) central and (b) forward rapidity regions.

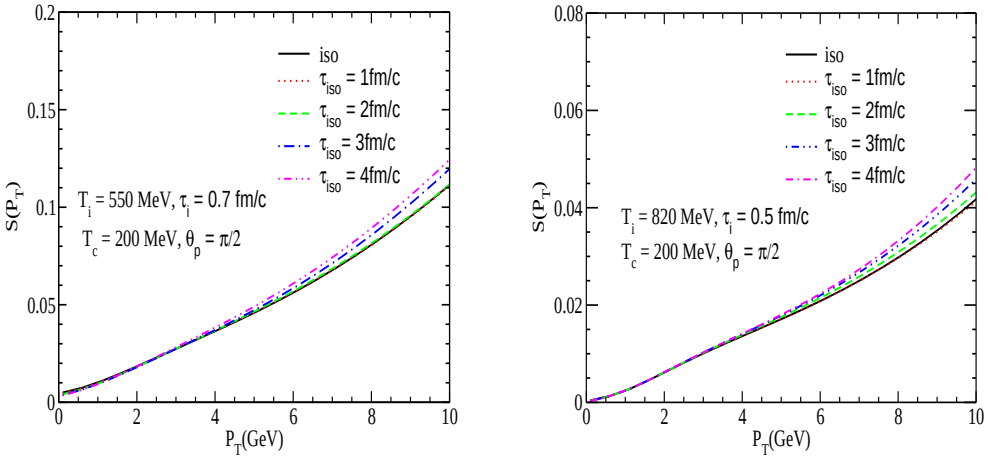

Figure 5.8: The survival probability of J/ψ in an anisotropic plasma at RHIC (Left panel) and LHC (right panel) energies with various value of the isotropization time $\tau_{\rm iso}$ at central rapidity.

$p_{\rm hard}$ = 300 MeV and for two different direction of propagation (θ_p) of the quarkonium with respect to the anisotropy axis. Again it is seen that the cross section first decreases with the anisotropy parameter upto $P_T \sim 5(3)$ GeV for $\theta_p = \pi/2(\pi/3)$ and we find larger

increase away from the central rapidity region.

Eq.(5.40) has been used to calculate the survival probability. Fig. 5.8 describes the survival probability of J/ψ for various values of the isotropization time $\tau_{\rm iso}$ at central rapidity region. Left (Right) panel corresponds to RHIC (LHC) energy. It is observed that the survival probability remains the same as in the isotropic case up to $P_T = 4$ GeV. Beyond that a marginal increase is observe with the increase of $\tau_{\rm iso}$.

5.4 Two-photon correlation in an anisotropic quark-gluon plasma

The method of two particle intensity interferometry, commonly known as Hanbury-Brown and Twiss (HBT) interferometry [165], is one of the effective technique to know the spatial and temporal information of particle emission zone created in high energy nucleus-nucleus collisions [166, 167, 168, 169, 170, 171]. It was first introduced in heavy ion collision in the hadronic sector through the study of quantum statistical correlation between identical pions which provided valuable information about the space-time description of the system at the freeze out surface [167]. In contrast to hadrons, the study of two-particle intensity interferometry of photons and dileptons [172, 173, 174, 175, 176, 177, 179, 180] which are produced throughout the space-time evolution of the reaction zone and which suffer almost no interactions with the surrounding medium can provide information of the history of the evolution of the hot matter created in heavy-ion collision.

The HBT effect differs from ordinary amplitude interferometry. The HBT effect is a consequence of quantum statistical effects resulting from the symmetrization of the wave function of bosons, or anti-symmetrization for fermions. In quantum mechanics, the interchange of two out of N indistinguishable bosons does not change the wave function. This feature of the Bose-Einstein correlation for the identical boson pairs results in the enhancement of the two-particle coincidence rate at small relative momentum of the pair. The measurement of the Bose-Einstein correlation is that it could provide not only the

extent of the source but also the emission duration of particle emission.

In this section, we present intensity interferometry with photon pair at most central RHIC initial conditions at $\sqrt{s_{NN}} = 200$ GeV including momentum anisotropy in the pre-equilibrium QGP phase. For the evolution in AQGP, the free streaming interpolating model with fixed initial condition has been used and relativistic (1+2)d hydrodynamical model with cylindrical symmetry and longitudinal boost invariance has been used for both isotropic QGP and hadronic phases. The thermalized isotropic QGP is assumed with sufficiently high energy densities at $\tau = \tau_{iso}$. Afterwards, with expansion, the energy density reduces, hadronization begins at τ_q (pure QGP phase ends here). The system then undergoes a phase transition at transition temperature (T_c) and transforms to a hadronic gas phase at τ_h. With further expansion, the energy density reduces further and finally reaches freeze-out at T_f, called freeze-out temperature at freeze-out time (τ_f).

5.4.1 Two particle correlation function

The two-particle correlation function is defined by the ratio of the two particle coincidence probability density over the product of the two single particle probabilities as

$$C_2 = \frac{P(\mathbf{p_1}, \mathbf{p_2})}{P(\mathbf{p_1})P(\mathbf{p_2})}, \tag{5.41}$$

where

$$P_1(\vec{k}) = \int d^4x \ \omega(x,k); \quad \omega(x,k) = E\frac{dR}{d^3k} \tag{5.42}$$

and

$$\begin{aligned} &P_2(\vec{k_1}, \vec{k_2}) = P_1(\vec{k_1})P_1(\vec{k_2}) \\ &+\frac{1}{2}\int d^4x_1 d^4x_2 \ \omega(x_1,K)\omega(x_2,K) \ \cos(\Delta x^\mu \Delta k_\mu), \end{aligned} \tag{5.43}$$

where $\omega(x,k)$ is the source function related to the thermal emission rate of the photon per unit volume and $\vec{k_i} = (k_{iT}\cos\psi_i, k_{iT}\sin\psi_i, k_{iT}\sinh y_i)$ is the three momentum of the

two identical photons with $i = 1, 2$, $K = (k_1 + k_2)/2$ is the average momentum, $\Delta k_\mu = k_{1\mu} - k_{2\mu} = q_\mu$, x_i and k_i are the four co-ordinates for position and momentum variables respectively and ψ_i's are the angles made by k_{iT} with the x-axis of each photon. The inclusion of the spin of the real photon will reduce the value of $C_2 - 1$ by 1/2. The source dimensions can be obtained by parameterizing the calculated correlation function with the empirical Gaussian form [166]:

$$C_2(q, K) = 1 + \lambda \exp(-R^2 q^2) \tag{5.44}$$

where λ is commonly referred as chaotic parameter, which varies from 0 to 1. Using the Bertsch-Patt parameterization, the correlation function can be written as a function of multi-dimensional HBT radii

$$C_2(q, K) = 1 + \lambda \exp(-R^2_{\rm side} q^2_{\rm side} - R^2_{\rm out} q^2_{\rm out} - R^2_{\rm long} q^2_{\rm long}). \tag{5.45}$$

The quantities $R_{\rm side}$, $R_{\rm out}$ and $R_{\rm long}$ are commonly known as HBT radii, which are the measures of Gaussian widths of the source size in $q_{\rm side}$, $q_{\rm out}$ and $q_{\rm long}$ direction. $q_{\rm side}$, $q_{\rm out}$ and $q_{\rm long}$ can be expressed in terms of individual particle momenta as:

$$\begin{aligned} q_{\rm side} &= \left| \vec{q_T} - q_{out} \frac{\vec{K_T}}{K_T} \right| \\ &= \frac{2k_{1T}k_{2T}\sqrt{1 - \cos^2(\psi_1 - \psi_2)}}{\sqrt{k^2_{1T} + k^2_{2T} + 2k_{1T}k_{2T}\cos(\psi_1 - \psi_2)}} \end{aligned} \tag{5.46}$$

$$\begin{aligned} q_{\rm out} &= \frac{\vec{q_T}.\vec{K_T}}{|K_T|} \\ &= \frac{(k^2_{1T} - k^2_{2T})}{\sqrt{k^2_{1T} + k^2_{2T} + 2k_{1T}k_{2T}\cos(\psi_1 - \psi_2)}} \end{aligned} \tag{5.47}$$

$$q_{\rm long} = k_{1z} - k_{2z} = k_{1T}\sinh y_1 - k_{2T}\sinh y_2 \tag{5.48}$$

where k_{iT} is the individual transverse momentum and y_i is the rapidity. The radius, $R_{\rm side}$, corresponding to $q_{\rm side}$ is closely related to the transverse size of the system. The radius, $R_{\rm out}$ corresponding to $q_{\rm out}$ measures both the transverse size and the duration of particle emission and $R_{\rm long}$ corresponding to $q_{\rm long}$ is the measure of longitudinal dimension of the system [167, 168, 169, 170, 171, 181, 182, 183].

5.4.2 Photon emission rate

A. Photon emission rate from AQGP

The lowest order processes for photon emission from QGP are the annihilation ($q\bar{q} \to g\gamma$) and Compton ($q(\bar{q})g \to q(\bar{q})\gamma$) processes. The total cross-section diverges in the limit $t/u \to 0$ which has been calculated considering the intermediate quarks acquires a thermal mass in the medium [184] to avoid the infrared divergence. The differential photon production rate for $1 + 2 \to 3 + \gamma$ processes in an anisotropic medium is given by [99, 100, 124]

$$E\frac{dR}{d^3k} = \frac{\mathcal{N}}{2(2\pi)^3}\int \frac{d^3p_1}{2E_1(2\pi)^3}\frac{d^3p_2}{2E_2(2\pi)^3}\frac{d^3p_3}{2E_3(2\pi)^3}(2\pi)^4\delta^{(4)}(p_1+p_2-p_3-k)\overline{|\mathcal{M}|^2} \times f_1(\mathbf{p}_1, p_{hard}, \xi) f_2(\mathbf{p}_2, p_{hard}, \xi)[1 \pm f_3(\mathbf{p}_3, p_{hard}, \xi)] \quad (5.49)$$

where $\mathcal{N}$ is the overall degeneracy of the corresponding process, $\overline{|\mathcal{M}|^2}$ is the square of the invariant amplitude for the processes [185] under consideration (here $q\bar{q} \to g\gamma$ and $qg \to q\gamma$), f_i's are the anisotropic distribution functions of the constituent partons in the medium. As the radial flow is not developed properly in the initial stage of the collision, its effect is neglected in the anisotropic phase. For $\tau_i \leq \tau \leq \tau_{iso}$, the system evolves anisotropically and it is described by free streaming interpolating model [131].

B. Photon emission rate from thermal medium

When $\tau_{iso} \leq \tau \leq \tau_f$, the system becomes thermalized and evolves hydrodynamically with energy density ($\mathcal{E}$) and velocity as a function of space and time. Hence, τ_{iso} is treated as free parameter in the calculation which controls the transition to the hydrodynamic scenario. Beyond $\tau \geq \tau_{iso}$, the system is described by ideal (1+2)d relativistic hydrodynamics

with longitudinal boost invariant and cylindrical symmetry. The rate of thermal photon production per unit space-time volume is given by [54, 186, 187, 188]:

$$E\frac{dR}{d^3k} = \frac{g^{\mu\nu}}{(2\pi)^3}\,\mathrm{Im}\Pi^R_{\mu\nu} f(E,T) \tag{5.50}$$

where $\mathrm{Im}\Pi^{\mu}_{\mu}$ is the imaginary part of the retarded photon self energy and $f(E,T)$ is the thermal phase space distribution. For an expanding system, the energy E should be replaced by $u_\mu k^\mu$, where k^μ and u^μ are the four momentum and the fluid four velocity respectively.

The initial condition are given through the energy density and the velocity profile,

$$\begin{aligned}
\mathcal{E}(\tau_i, r) &= \frac{\mathcal{E}_0\,(\xi=0, T_i^{\mathrm{hydro}})}{1+\exp(\frac{r-R_T}{\sigma})} \\
v_r(\tau_i, r) &= v_0\left(1 - \frac{\mathcal{E}_0\,(\xi=0, T_i^{\mathrm{hydro}})}{1+\exp(\frac{r-R_T}{\sigma})}\right)
\end{aligned} \tag{5.51}$$

where $\mathcal{E}_0\,(\xi=0, T_i^{\mathrm{hydro}})$ is the initial energy density which is related to initial temperature T_i^{hydro} and it can be obtained by the relation $T_i^{\mathrm{hydro}} = p_{\mathrm{hard}}(\tau_{\mathrm{iso}})$ [99]. R_A is the nuclear radius and σ is the diffusion parameter and taken as 0.5 fm. For the QGP and the hadronic phases lattice QCD EoS [189] (for $T > T_c$) and hadronic resonance gas EoS [190] (for $T < T_c$) have been used respectively. For the transition region we have used the following parameterization [191];

$$\begin{aligned}
s(T) &= s_q(T) f_q(T) + [1 - f_q(T)] s_h(T), \\
f_q(T) &= \frac{1}{2}(1 + \tanh\frac{T - T_c}{\Gamma})
\end{aligned} \tag{5.52}$$

where Γ is the width parameter and assumes a finite value for the crossover transition and for the first order transition this value can be tuned to zero. Here the width parameter is taken to be Γ=25 MeV.

Therefore, the one- and two- particle inclusive spectra can be presented as follows,

$$\begin{aligned}
P_1(k) &= P_1^{\mathrm{aniso}}(k) + P_1^{\mathrm{hydro}}(k) \\
P_2(k_1,k_2) &= P_2^{\mathrm{aniso}}(k_1,k_2) + P_2^{\mathrm{hydro}}(k_1,k_2)
\end{aligned} \tag{5.53}$$

$P_i^{\rm aniso}$ and $P_i^{\rm hydro}$ can be evaluated using Eqs. (5.42) and (5.43) with the help of space-time prescription for anisotropic and hydrodynamic scenario discussed earlier. Finally using Eq. (5.41) we obtain C_2 for the full evolution as well as for the individual phases.

5.4.3 Results

Now, we evaluate the correlation function, C_2 as a function of $q_{\rm out}$, $q_{\rm side}$ and $q_{\rm long}$ for two sets of RHIC initial conditions. For central $Au + Au$ collisions at RHIC we take initial temperature T_i = 446 MeV and initial time τ_i = 0.147 fm/c for SET-I and T_i = 350 and τ_i = 0.24 fm/c for SET-II. We fix the transition temperature T_c = 175 MeV and the freeze-out temperature T_f = 120 MeV. We choose $\tau_{\rm iso}$ in such a way that one of the values corresponds to the isotropic situation ($\tau_{\rm iso} = \tau_i$) and others corresponds to anisotropic scenario ($\tau_{\rm iso} > \tau_i$). So basically we have attempted to examine the sensitivity of momentum anisotropy on C_2 by controlling the variable, $\tau_{\rm iso}$.

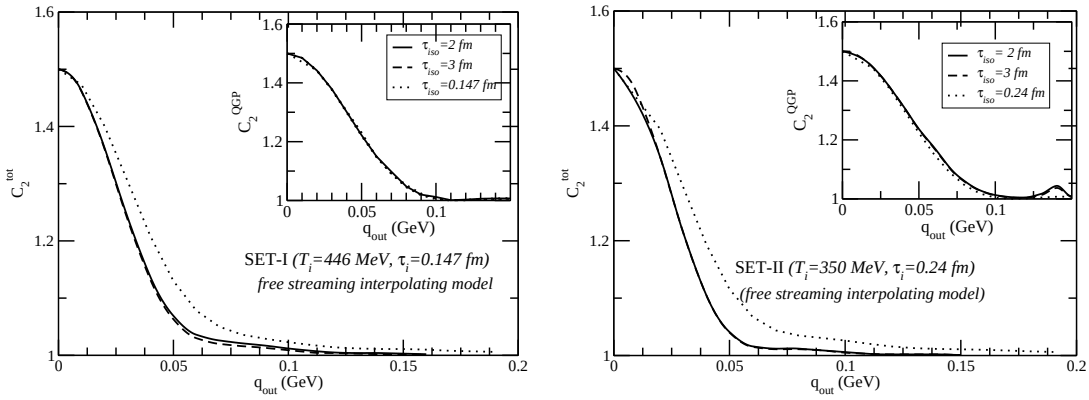

Figure 5.9: Correlation function for photon pairs as a function of $q_{\rm out}$ for SET-I (left) and SET-II (right) are plotted with different $\tau_{\rm iso}$ and the inset figure is same for QGP (aQGP+iQGP) phase only.

C_2 as function of q_{out} is calculated by taking $\psi_1 = \psi_2$=0, $y_1 = y_2$=0 and fixing transverse momentum of one photon (k_{1T} = 2 GeV) and varying the other (k_{2T}). In Fig. 5.9, we have plotted the variation of C_2 as a function of $q_{\rm out}$ in full evolution scenario for two set of RHIC

initial conditions. From both the figures, we infer that varying $\tau_{\rm iso}$, a considerable shift is observed in C_2. By increasing $\tau_{\rm iso}$, the value of $R_{\rm out}$ (see table 5.1) which corresponds to $q_{\rm out}$ increases. This happens because by increasing $\tau_{\rm iso}$, the system expands slower to achieve thermalization and isotropization. Whereas C_2 for the QGP (aQGP+isotropic QGP) phase depicted in the insets of Fig. 5.9, substantial change is not observed, unlike the case for $C_2^{\rm tot}$. This happens because the flow is not developed in early QGP phase and with the progress of time the thermal energy is transformed into flow energy in later stage of the collision, so flow is fully developed in the hadronic stage [178, 179] resulting in reduction of $R_{\rm out}$ by increasing $\tau_{\rm iso}$. The reduction is mostly affected due to the radial flow as well as the $\tau_{\rm iso}$ dependent initial conditions for hydrodynamic evolution which is due to the inclusion of momentum space anisotropy.

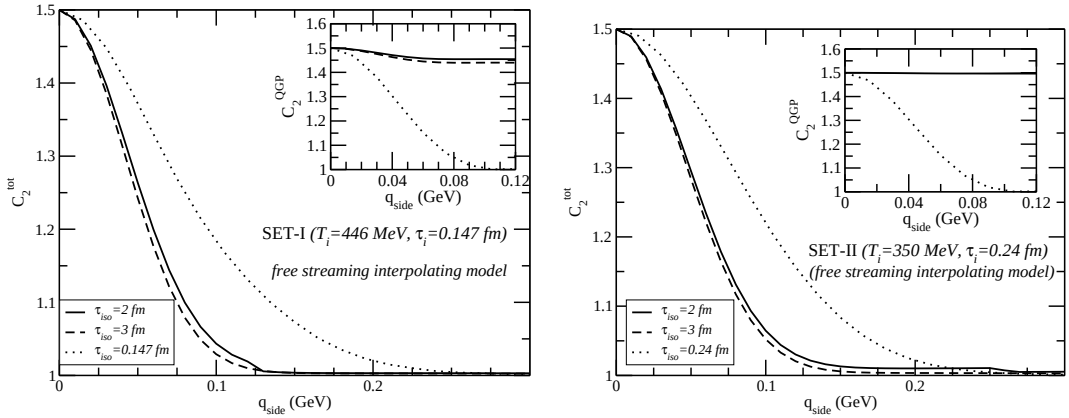

Figure 5.10: Correlation function for photon pairs as a function of $q_{\rm side}$ for SET-I (left) and SET-II (right) are plotted with different $\tau_{\rm iso}$ and the inset figure is same for QGP (aQGP+iQGP) phase only.

By taking $k_{1T} = k_{2T} = 2$ GeV, $y_1 = y_2$=0 and fixing ψ_2=0 and varying ψ_1, we obtain C_2 as a function of $q_{\rm side}$. In Fig. 5.10 we display the variation of C_2 as a function of $q_{\rm side}$ for the full evolution scenario for two set of RHIC initial conditions. With increasing $\tau_{\rm iso}$, the value of $R_{\rm side}$ (see table 5.1) which corresponds to $q_{\rm side}$ is also enhanced. This happens because by

increasing $\tau_{\rm iso}$, the system expands slower to achieve thermalization and isotropization. By increasing $\tau_{\rm iso}$ the values of $R_{\rm side}$ increase in full evolution scenario whereas it decrease in the QGP phase. It can be shown that $R_{\rm side} \sim 1/(1+E_{\rm collective}/E_{\rm thermal})$ [166], where $E_{\rm thermal}$ depends inversely on $\tau_{\rm iso}$. In addition to it, the flow is not developed properly in the QGP phase, so $E_{\rm collective} \ll E_{\rm thermal}$. Thus, with the increase of $\tau_{\rm iso}$ the ratio $E_{\rm collective}/E_{\rm thermal}$ increases. As a result the value of $R_{\rm side}$ decreases. Whereas in the hadronic phase, the flow is fully developed resulting in $E_{\rm collective} \gg E_{\rm thermal}$. The thermal energy is reduced even more by increasing $\tau_{\rm iso}$. So due to the radial flow effect the values of $R_{\rm side}$ increase with the increase in the values of $\tau_{\rm iso}$ in the full evolution scenario.

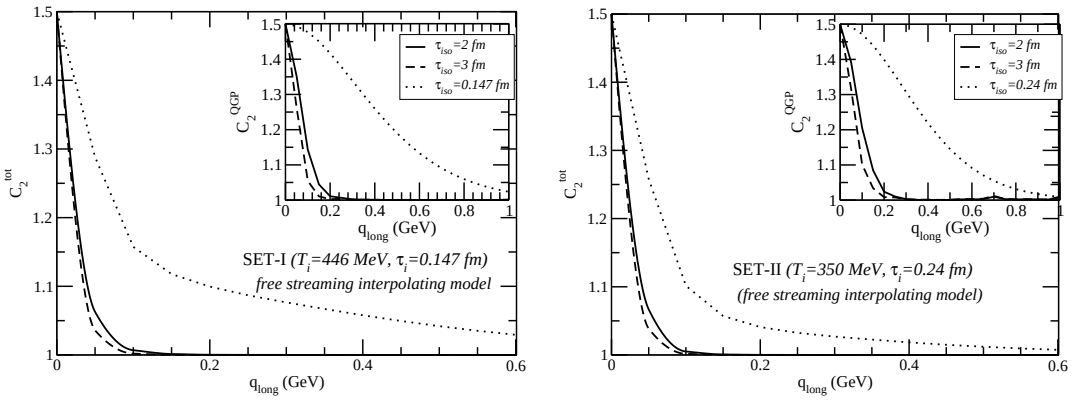

Figure 5.11: Correlation function for photon pairs as a function of $q_{\rm long}$ for SET-I (left) and SET-II (right) are plotted with different $\tau_{\rm iso}$ and the inset figure is same for QGP (aQGP+iQGP) phase only.

By taking $\psi_1 = \psi_2$=0, $k_{1T} = k_{2T}$=2 GeV and taking one of the photons at mid-rapidity ($y_1 = 0$) and varying the other (y_2), we obtain C_2 as a function of $q_{\rm long}$. The variation of C_2 as a function of $q_{\rm long}$ with SET-I and SET-II initial conditions for RHIC energy is shown in Fig. 5.11. It is clear from both the figures that there is a considerable difference for isotropic (when $\tau_{\rm iso} = \tau_i$) and anisotropic (for $\tau_{\rm iso}$= 2, 3 fm/c) scenarios. It is argued previously that the anisotropy in momentum space arises due to $< p_L^2 > \ll < p_T^2 >$. Thus we can argue here that the difference arises in size in the longitudinal direction because of

the above said asymmetry in momentum space. Hence $R_{\rm long}$ increases (see Table 5.1) with the increase of $\tau_{\rm iso}$.

The HBT radii obtained from C_2 using Eq. 5.45 is tabulated in Table. 5.1. It is clear that the HBT radii increase with the inclusion of anisotropy, i.e., with increasing $\tau_{\rm iso}$. Also a remarkable change in HBT radii is observed in the QGP phase (for both R_{side} and R_{long}) with the inclusion of momentum space anisotropy except the outward direction.

Table 5.1: The values of $R_{\rm out}$, $R_{\rm side}$ and $R_{\rm long}$ obtained from C_2 (using Eq. 5.45) is tabulated below.

T_i (MeV)	$\tau_{\rm iso}(fm/c)$	$R_{\rm out}$ (fm)	$R_{\rm side}$ (fm)	$R_{\rm long}$ (fm)
446	0.147	4.5	1.95	2.6
	2.0	5.5	3.13	6.6
	3.0	5.6	3.34	6.8
350	0.24	4.69	1.77	2.9
	2	6.08	2.83	6.3
	3	6.09	2.96	6.7

5.5 Conclusion

In presence of the initial state of anisotropy, the radiative energy loss increases by a factor $1.2-2.0$ depending upon the value of anisotropy parameter ξ and direction of the propagation of the parton with respect to the anisotropy axis. It affects the hadron p_T spectrum. The result of the nuclear modification factor for two different values of $\tau_{\rm iso}$ are compared with the PHEHIX data. It is found that for FIC, the data is well reproduced if $\tau_{\rm iso}$ lies between $0.5-1.5$ fm/c. We also observed that for lower initial temperature the upper limit of the extracted value of $\tau_{\rm iso}$ is slightly higher as compared to the case where the large value of initial temperature is used.

It is to be noted that we have not incorporated the collisional energy loss assuming that the contribution will be subleading. However, a complete calculation must include both the energy loss mechanisms in order to extract $\tau_{\rm iso}$.

We have calculated the gluon J/ψ dissociation cross section in an anisotropic QGP expected to be formed in relativistic nucleus-nucleus collision. It is shown that the thermally weighted cross section is modified substantially in anisotropic plasma. It is seen that the cross section first decreases with ξ and then increases as compared to the isotropic case. It is also seen that depending upon the initial conditions, the survival probability in anisotropic QGP marginally differs from that in the isotropic QGP for both central as well as forward rapidity region.

We have studied the intensity correlation for the photons at most central collision at RHIC energies to obtain the space-time structure of heavy-ion collision. In this work, we have evaluated the correlation function C_2 for two real photons as functions of $q_{\rm out}$, $q_{\rm side}$ and $q_{\rm long}$ with the initial state momentum space anisotropy. Hence, $R_{\rm out}$, $R_{\rm side}$ and $R_{\rm long}$ extracted from Bose-Einstein correlation function, C_2 in such a scenario provide us with the special information of the evolving system. For the entire evaluation, we do observe that the value of C_2 as function of the q's is reduced for the anisotropic case compared to that of isotropic case in all the direction. The large variation of C_2 is obtained along the longitudinal direction because of the asymmetry in the $p_T - p_L$ plane. Therefore, the maximum effect of momentum anisotropy is observed in $R_{\rm long}$ and the corresponding values change quite substantially with $\tau_{\rm iso}$ for both sets of initial conditions.

• ○ •

Chapter 6

Conclusions and Outlook

The cardinal focus of this work is to explore the characteristic of the pre-equilibrium quark-gluon plasma, as created in heavy-ion collision. We started with an introduction to the field of research relevant to this thesis. At first, we have introduced the kinetic theory for non-Abelian plasmas, which is an ideal tool to investigate plasma instability. Within the framework of kinetic theory, we have investigated the wake in charge density and the wake potential due to a passage of fast partons traveling through the high temperature QCD plasma which is anisotropic in momentum space. It has been shown that in an anisotropic plasma, the wake in induced charge density indicates a little oscillatory behavior when the parton moves along the anisotropy direction ($\hat{n}$) and the parton velocity remains below the phase velocity ($v < v_p$), contrary to the isotropic case. With the jet velocity greater than the phase velocity, the oscillatory behavior increases with ξ. The wake potential shows a decrease of negative minimum in presence of anisotropy. On the other hand, when the velocity of jet is perpendicular to the anisotropy direction, the oscillatory nature of the color charge wake is reduced at $v > v_p$. As a consequence, we do not observe any oscillatory nature of the wake potential in the backward direction at large value of ξ. Further, we extended our calculation to include the collision term in the Boltzmann transport equation. Collisions, being responsible for the fast thermalization are needed to reach the equilibrium state of maximum entropy. We investigated the effect of collisions on the wake potential in

an anisotropic plasma. It was shown that in a collisional anisotropic plasma, the oscillatory behavior of the wake potential is smeared out and also if we increase the collision frequency, the depth of the potential becomes highest when the parton moves along the parallel direction. When $\mathbf{r} \perp \mathbf{v}$, the wake potential turns into a modified Coulomb-like potential for collisional plasma.

In the early stage of the non-central heavy-ion collision, a very strong magnetic field is generated due to the presence of charge species. Therefore, it is important to understand the properties of the QCD plasma under strong magnetic field. The effect of the magnetic field on the collective modes of QGP has been investigated [192] recently and there exist an unstable mode, signaling the presence of plasma instability. The effect of strong magnetic field on the wake is an important problem to be addressed.

The characteristic behavior of collective modes of a system composed by relativistic jets in a collisionless anisotropic quark gluon plasma has been examined in detail. At very short time scales after the interaction between the jet and the anisotropic plasma sets in we find that the growth of the unstable mode very much depends on the strength of the jet (η) and anisotropy parameter ξ. In the weak coupling regime, we found the plasma instability was fully developed on time scale of the order of $t \sim 1 - 3$ fm/c at plasma temperature $T \sim 350$ MeV.

In our calculation, we have assumed that the jet of particles can be represented as a delta-like distribution function. In the most realistic situation in heavy-ion collision, the distribution function of jet is more complicated. We have also neglected the effect of collision. Indeed if the instability is not saturated due to non-Abelian effect, the collision term will probably stop their growth anyway. Furthermore, in heavy-ion collision, two jets of particles propagate in opposite direction in an anisotropic plasma, which however relevant to calculate the plasma instability. Thus, the consideration of all the above mentioned effects is required to compute the complete scenario of the jet medium interaction mechanism.

In the investigation of the probes of pre-equilibrium situation, we studied the effect of plasma anisotropy on the nuclear modification factor (R_{AA}) of light hadron, gluon dissociation of J/ψ and two photon interferometry. We have shown in the text that the presence of pre-equilibrium anisotropy increases the radiative energy loss by a factor 1.2 -2 depending upon the propagation of parton along the direction of anisotropy and anisotropy parameter ξ. It has also been argued in the text that for FIC, the PHENIX data are well reproduce if isotropization time lies in the range $0.5 \leq \tau_{\rm iso} \leq 1.5$ fm/c. But, the present model is unable to predict the isotropization time at LHC energies. We have also shown in the text that the thermally weighted cross section is modified substantially in anisotropic plasma whereas effect on the survival probability of J/ψ is negligible. Furthermore, we have attempted to estimate the correlation function, C_2 for two identical photons as a functions of $q_{\rm out}$, $q_{\rm side}$ and $q_{\rm long}$ for RHIC energies. One of the interesting finding of the present work has been the variation of C_2 along the longitudinal direction because of the asymmetry in the momentum space and correspondingly $R_{\rm long}$ changes quite substantially with $\tau_{\rm iso}$.

An alternative framework for describing dissipative dynamics is needed to describe the dynamics of highly momentum space anisotropy. Anisotropic hydrodynamics (aHYDRO) is quite successful in the recent years [193], which is based on the reorganization of the hydrodynamics expansion around the anisotropic background. The necessary aHYDRO dynamical equations are derived by taking moments of the Boltzmann equation using a momentum space anisotropy one particle distribution function which can be expressed in the form

$$f(x,p) = f_{\rm iso}\left(\frac{\sqrt{p^{\mu}\Sigma_{\mu\nu}(x)p^{\nu}}}{\Lambda(x)}, \frac{\mu(x)}{\Lambda(x)}\right) \tag{6.1}$$

where $\Sigma_{\mu\nu}(x)$ is a symmetric tensor that measures the momentum space anisotropy, $f_{\rm iso}$ is an arbitrary isotropic distribution function and $\Lambda(x)$ is the momentum scale. The aHYDRO framework is more accurately describes the early time dynamics of the QGP created in heavy-ion collision and temperature dependent $\eta/\mathbf{S}$. In the future, the aHYDRO will be used to understand the properties of the QGP and study the signature of the QGP.

Bibliography

[1] D. J. Gross and F. Wilczek, *Phys. Rev. Lett.* **30** 1343–1346 (1973).

[2] H. D. Politzer, *Phys. Rev. Lett.* **30** 1346–1349 (1973).

[3] E. V. Shuryak, *Sov. Phys. JETP* **47** 212–219 (1978).

[4] E. V. Shuryak, *Phys. Lett.* **B78** 150 (1978).

[5] O. K. Kalashnikov and V. V. Klimov, *Phys. Lett.* **B88** 328 (1979).

[6] J. I. Kapusta, *Nucl. Phys.* **B148** 461–498 (1979).

[7] E. V. Shuryak, *Phys. Rept.* **61** 71–158 (1980).

[8] H. G. Baumgardt et al., *Z. Phys. A* **273**, 359 (1975).

[9] E. W. Kolb and M. S. Turner, *The Early Universe*, Westview Press, 1990

[10] N. K. Glendenning, *Phys. Rept.* **342**, 393 (2001).

[11] A. Chodos, R. L. Jaffe, K. Jhonson, C. B. Thorn, V. F. Weisskopf, *Phys. Rev. D* **9**, 3471 (1974).

[12] A. Chodos, R. L. Jaffe, K. Jhonson, C. B. Thorn, Phys. Rev. D **10**, 2599 (1974).

[13] T. De. Grande, R. L. Jaffe, K. Jhonson, J. Kiskis, Phys. Rev. D **12**, 2060 (1975).

[14] C. R. Allton et al., Phys. Rev. D **68** (2003) 014507,

[15] F. Karsch, E. Laermann, and A. Peikert, Phys. Lett. **B478** (2000) 447.

[16] F. Karsch, Lattice qcd at high temperature and density, Lect. Notes Phys. **583** (2002) 209.

[17] F. Karsch, Nucl. Phys. A **698**, 199 (2002).

[18] T. D. Lee and G. C. Wick, Phys. Rev. D **9**, 2291 (1974).

[19] J. D. Bjorken, Phys. Rev. D **27** (1983) 140.

[20] J. D. Bjorken, Fermilab-Pub-82/59-THY(1982) and Erratum (Unpublished).

[21] M. Gyulassy, P. Levai and I. Vitev, Nucl. Phys. B **571**, 197 (2000).

[22] B. G. Zakharov, JETP Lett. **73**, 49 (2001).

[23] M. Djordjevic and U. Heinz, Phys. Rev. Lett. **101**, 022302 (2008).

[24] R. Baier *et al.*, J. High Ener. Phys. **0109**, 033 (2001)

[25] S. Jeon and G. D. Moore, Phys. Rev. C **71**, 034901 (2005).

[26] A. K. Dutt-Mazumder, J. Alam, P. Roy, and B. Sinha, Phys. Rev. D **71**, 094016 (2005).

[27] P. Roy, J. Alam, and A. K. Dutt-Mazumder, J. Phys. G. **35**, 104047 (2008).

[28] S. S. Adler *et al.* (PHENIX Collaboration), Phys. Rev. Lett. **94**, (2005) 232301.

[29] J. Adams *et al.* (STAR Collaboration), Phys. Rev. Lett. **91**, (2003) 172302.

[30] K. Aamodt *et al.* (ALICE Collaboration), Phys. Rev. Lett. **106**, (2011), 032301.

[31] K. Aamodt *et al.* (ALICE Collaboration), Phys. Lett. **B696**, 30 (2011).

[32] H. Satz and T. Matsui, Phys. Lett. **B178**, 416 (1986).

[33] X. M. Xu, D. Kharzeev, H. Satz, and X. N. Wang, Phys. Rev. C **53**, 3051 (1996).

[34] B. Alessandro *et al.* (NA50 Collaboration), Eur. Phys. J. C **39**, 335 (2005).

[35] A. Adare *et al.* (PHENIX Collaboration), Phys. Rev. Lett. **98**, 232301 (2007).

[36] G. Aad *et al.* (Atlas Collaboration), Phys. Lett. **B697**, 294 (2011).

[37] J. Rafelski, R. Hagedorn: "*From Hadron Gas to Quark Matter 2*" (1981).

[38] J. Rafelski, B. Müller, Phys. Rev Lett. **48** 1066 (1982).

[39] Giorgio Torrier, J. Phys. G: Nucl. Part. Phys. **36**, (2009) 064007.

[40] K. Kajantie and H. I. Miettinen, Zeit. Phys. C **9**, (1981) 341.

[41] F. Halzen and H. C. Liu, Phys. Rev. D **25**, (1982) 1842.

[42] B. Sinha, Phys. Lett. **B128**, (1983) 91.

[43] R. C. Hwa and K. Kajantie, Phys. Rev. D **32**, (1985) 1109.

[44] G. Staadt, W. Greiner, and J. Rafelski, Phys. Rev. D **33**, (1986) 66.

[45] M. Neubert, Z. Phys. C **42** (1989) 231242.

[46] J. I. Kapusta, P. Lichard, and D. Seibert, Phys. Rev. D **44** (1991) 2774, Erratum ibid **47**, 4171 (1993).

[47] J. Alam, S. Sarkar, P. Roy, T. Hatsuda and B. Sinha, Ann. Phys.**286**, (2001) 159.

[48] P. K. Roy, D. Pal, S. Sarkar, D. K. Srivastava, and B. Sinha, Phys. Rev. C **53** 2364 (1996).

[49] P. Arnold, G. D. Moore and L. G. Yaffe, JHEP 0112, 009 (2001).

[50] K. Kajantie, J. Kapusta, L. Mclerran, A. Mekjian, Phys. Rev. D **34**, 2746 (1986).

[51] K. J. Eskola and J. Lindfors, Z. Phys. C **46**, 141 (1990).

[52] K. Geiger and J. I. Kapusta, Phys. Rev. Lett. **70** 1920 (1993).

[53] S. Chakraborty, J. Alam, D. K. Srivastava, S. Raha, and B. Sinha, Phys. Rev. D **46**, (1992) 3802.

[54] H. A. Weldon,Phys. Rev. D **42**, (1990) 2384.

[55] C. Gale and J. I. Kapusta, Nucl. Phys. B**357**, (1991) 6589.

[56] R. Rapp, G. Chanfray, and J. Wambach,Phys. Rev. Lett. **76**, (1996) 368.

[57] R. Rapp and J. Wambach, Adv. Nucl. Phys. **25**, (2000).

[58] T. Renk, R. A. Schneider, and W. Weise, Phys. Rev. C **66** (2002) 014902.

[59] J. Ruppert, T. Renk, and B. Muller, Phys. Rev. C **73**, (2006) 034907,

[60] B. Schenke and C. Greiner, Phys. Rev. C **73**, (2006) 034909,

[61] F. Retiere, J. Phys. G **30**, (2004) S827S834.

[62] A. M. Poskanzer and S. A. Voloshin, Phys. Rev. C **58**, (1998) 16711678.

[63] P. Huovinen,P. F. Kolb, U. W. Heinz, P. V. Ruuskanen, and S. A. Voloshin Phys. Lett. **B503** (2001) 58.

[64] T. Hirano, and K. Tsuda, Phys. Rev. C **66**, 054905

[65] R. Baier, A. H. Mueller, D. Schiff, and D. T. Son, Phys. Lett. **B502**, (2001) 5158

[66] E. Shuryak, J. Phys. G **30**, (2004) S1221S1224.

[67] M. Luzum and P. Romatschke, Phys. Rev. C **78**, 034915 (2008)

[68] S. Mrowczynski, Phys. Lett. **B314**, (1993) 118121.

[69] S. Mrowczynski, Phys. Rev. C **49**, (1994) 21912197.

[70] J. Randrup and S. Mrowczynski, Phys. Rev. C **68**, (2003) 034909.

[71] P. Romatschke and M. Strickland, Phys. Rev. D **68**, (2003) 036004.

[72] P. Arnold, J. Lenaghan, and G. D. Moore, JHEP 08 (2003) 002.

[73] A. Dumitru and Y. Nara, Qcd plasma instabilities and isotropization,Phys. Lett. **B621** (2005) 89.

[74] D. Moore, and L. G. Yaffe Phys. Rev. Lett. **94**, 072302 (2005).

[75] A. Rebhan, P. Romatschke, and M. Strickland, Phys. Rev. Lett. **94**, (2005) 102303.

[76] J. Adams *et al.* (STAR Collaboration), Phys. Rev. Lett. **95**, (2005) 152301.

[77] S. S. Adler *et al.* (PHENIX Collaboration), Phys. Rev. Lett. **97**, (2006) 052301.

[78] H. A. Weldon, Phys. Rev. D **26** (1982) 1394.

[79] M. Le Bellac, Thermal Field Theory (Cambridge University Press, Cambridge, England, 1996).

[80] J.-P. Blaizot and E. Iancu, Phys. Rept. **359**, (2002) 355.

[81] H. T. Else and U. Heinz, Phys. Rep. **183**, (1989) 81.

[82] H.-TH. Elze, D. Vasak, and M. Gyulassy, Nucl. Phys. B**276**, 706 (1986).

[83] S. Mrowczynski, Phys. Rev. D **39**, 1940 (1989).

[84] J. P. Blaizot and E. Iancu, Phys. Rev. Lett. **70**, 3376 (1993).

[85] P. F. Kelly, Q. Liu, C. Lucchesi, and C. Manuel, Phys. Rev. D **50**, 4209 (1994).

[86] J.-P. Blaizot and E. Iancu, Nucl. Phys. B**557**, 183 (1999).

[87] S. Mrowczynski, Phys. Lett. **B393**, 26 (1997).

[88] S. Mrowczynski and M. H. Thoma, Phys. Rev. D **62**, 036011 (2000).

[89] J. Randrup and S. Mrowczynski, Phys. Rev. C **68**, 034909 (2003).

[90] B. Schenke, M. Strickland, C. Greiner, and M. H. Thoma, Phys. Rev. D **73**, 125004 (2006).

[91] M. Mandal, and P. Roy, Phys. Rev. D **88** 074013 (2013).

[92] S. Mrowczynski, Acta. Phys. Pol. B **37**, 427 (2006);

[93] P. Romatschke and R. venugopalan, Phys. Rev. Lett. **96**, 062302 (2006).

[94] M. Strickland, J. Phys. G **34**, S429 (2007).

[95] M. Strickland, and P. Romatschke, Phys. Rev. D **70**, 116006 (2004).

[96] P. Arnold, G. D. Moore, and L. G. Yaffe, Phys. Rev. D **72**, 054003 (2005).

[97] P. Arnold, P. Romatschke, and M. Strickland, JHEP 09, 041 (2005).

[98] B. Schenke, and M. Strickland Phys. Rev. D **74**, 065004 (2006).

[99] L. Bhattacharya and P. Roy, Phys. Rev C **78**, 064904 (2008).

[100] L. Bhattacharya and P. Roy, Phys. Rev C **79**, 054910 (2009).

[101] B. Schenke "Collective Phenomena in the Non-Equilibrium Quark-Gluon Plasma" PhD Thesis.

[102] M. Strickland, Braz. J. Phys. **37**, 762 (2007)

[103] E. Webel, Phys. Rev. Lett. **2**, 83 (1959)

[104] V. Greco, C. M. Ko and P. Levai, Phys Rev. Lett. **90**, 202302 (2003); Phys. Rev. C **68**, 034904 (2003).

[105] R. C. Hwa and C. B. Yang, Phys. Rev. C **70**, 024905 (2004); J. Phys. G **30** S1117 (2004).

[106] J. Casalderrey-Solana, E. V. Shuryak and D. Teaney, J. Conf. Ser. **27**, 22 (2005).

[107] J. Casalderrey-Solana, J. Phys. G **34** S345 (2007).

[108] H. Stoecker Nucl. Phys. A **750**, 121 (2005).

[109] V. Koch, A. Majumder and Xin-Nian Wang, Phys. Rev. Lett. **96**, 172302 (2006).

[110] A. Majumder and Xin-Nian-Wang, Phys. Rev. C **73**, 051901 (2006).

[111] J. Ruppert and B. Muller Phys. Lett. **B618**, 123 (2005).

[112] J. Ruppert and B. Muller, Nucl. Phys. A **774**, 397 (2006).

[113] P. Chakraborty, M. G. Mustafa and M. H. Thoma, Phys. Rev. D **74**, 094002 (2006).

[114] P. Chakraborty, et al., J. Phys. G **34**, 2141 (2007).

[115] Bing-feng Jiang, Jia-rong Li, Nucl. Phys. A **856**, 121 (2011). J. Phys. G **39**, 025007 (2012).

[116] M. Mandal and P. Roy, Phys. Rev. D **86**, 114002 (20012).

[117] S. Ichimaru, Basic Principles of Plasma Physics (W. A. Benjamin, INC. 1973).

[118] N. A. Krall and A. W. Trivilpiece, Principles of Plasma Physics (New York: McGraw-Hill).

[119] L. D. Landau, E. M. Lifshitz, Fluid Mechanics, 2nd edition.

[120] M. C.Chu and T. Matsui, Phys. Rev. D **39**, 1892 (1989).

[121] I. M. Dremin, Nucl. Phys. A **767**, 233 (2006).

[122] W. J. Miloch, Plasma Phys. Control. Fusion **52**, (2010) 124004.

[123] P. L. Bhatnagar, E. P. Gross, and M Krook, Phys. Rev. **94**, 511 (1954).

[124] B. Schenke, M. Strickland, Phys. Rev. D **76**, 025023 (2007).

[125] M. E. Carrington, T. Fugleberg, D. Pickering and M. H. Thoma Can. J. Phys. **82**, 671 (2004).

[126] C. Manuel and S. Mrowczynski, Phys. Rev. D **74**, 105003 (2006).

[127] M. Mannarelli and C. Manuel, Phys. Rev. D **76**, 094007 (2007).

[128] M. Mannarelli and C. Manuel, Phys. Rev. D **77**, 054018 (2008).

[129] M. Mannarelli, C. Manuel, S. Gonzalez-Solis and M. Strickland, Phys. Rev. D **81**, 074036 (2010).

[130] M. Mandal, and P. Roy, Phys. Rev. D **89**, 074016 (2014).

[131] M. Martinez and M. Strickland, Phys. Rev. Lett. **100**, 102301 (2008).

[132] M. Mandal, and P. Roy, Adv.High Energy Phys. **2013**, 1 (2013).

[133] R. D. Pisarski, arXiv: hep-ph/9710370.

[134] M. Martinez and M. Strickland, Phys. Rev. C **78**, 034917 (2008).

[135] M. Martinez and M. Strickland, Eur. Phys. J. **C61**, 905 (2009).

[136] M. Martinez and M. Strickland, Phys. Rev. C **79**, 044903 (2009).

[137] L. Bhattacharya, and P. Roy, Phys. Rev. C **81**, 054904 (2010).

[138] L. Bhattacharya, and P. Roy, J. Phys. G **37**, 105010 (2010).

[139] M. Strickland, Pramana **84**, 671 (2015).

[140] A. Mukherjee, M. Mandal, and P. Roy, arXiV **1604.08313** [hep-ph](2016).

[141] P. Romatschke, M. Strickland, Phys. Rev. D **71**, 125008 (2005).

[142] M. Mandal, S. Sarkar, P. Roy, and A. Dutt-Majumder arXiv **1109.1181** [**hep-ph**] (2011).

[143] P. Roy, and A. K. Dutt-Mazumder, Phys. Rev. C **83**, 044904 (2011).

[144] M. Mandal, L. Bhattacharya, and P. Roy, Phys. Rev. C **84**, 044910 (2011).

[145] M. Mandal, and P. Roy, Phys. Rev. C **86**, 024915 (2012).

[146] G. D. Moore, and D. Teaney, Phys. Rev. C **71**, 064904 (2005).

[147] P. Romatschke, Phys. Rev. C **75**, 014901 (2007).

[148] A. Dumitru, Y. Nara, B. Schenke, and M. Strickland, Phys. Rev. C **78**, 024909 (2008).

[149] P. Mohanty, M. Mandal and P. Roy Phys. Rev. C **89**, 054915 (2014).

[150] T. Renk, Phys. Rev. C **71**, 064905 (2005).

[151] M. Gyulassy, I. Vitev, X. N. Wang, and P. Huovinen, Phys. Lett. **B526**, 301 (2002).

[152] S. turbide, C. Gale, S. Jeon, and G. D. Moore, Phys. Rev. C **72**, 014906 (2005).

[153] P. Romatschke and M. strickland, Phys. Rev. D **69**, 065005 (2005).

[154] M. Djordjevic, **Phys. Rev. C 80**, 064909 (2009).

[155] M. Gyulassy and X. N. Wang, Nucl. Phys. **B420**, 583 (1994).

[156] R. Baier and Y. Mehtar-Tani, Phys. Rev. C **78**, 064906 (2008).

[157] A. Dumitru, Y. Guo, and M. Strickland, Phys. Lett. **B662**, 37 (2008).

[158] J. F. Owens, Rev. Mod. Phys. **59**, 465 (1987).

[159] X. N. Wang, Phys. Rev. C **58**, 2321 (1998).

[160] P. Roy, A. K. Dutt-Mazumder and J. Alam, Phys. Rev. C **73**, 044911 (2006).

[161] S. S. Adler *et al.*, (PHENIX Collaboration), Phys. Rev. Lett. **96** (2006) 202301.

[162] G. Bhanot amd M. E. Peskin, Nucl. Phys. **B156**, 391 (1979).

[163] D. Kharzeev and H. Satz, Quark-Gluon Plasma II, edited by R. C. Hwa (world scientific Singapore 1995).

[164] M. Margotta, K. McCarty, C. McGahan, M. Strickland, and D. Yager-Elorriaga, Phys. Rev. **D83**, 105019 (2011).

[165] R. Hanbury Brown and R. Q. Twiss, Nature **178**, 1046(1956).

[166] S. Pratt, Phys. Rev. D **33**, 1314 (1986).

[167] U. A. Weidemann and U. Heinz, Phys. Rep. **319**, 145 (1999).

[168] U. Heinz and B. V. Jacak, Ann. Rev. Nucl. Part. Sci. **49**, 529 (1999).

[169] T. Csörgo and B. Lörstad, Phys. Rev. C **54**, 1390 (1996).

[170] B. R. Schlei and N. Xu, Phys. Rev. C **54**, R2155 (1996).

[171] D. H. Rischke and M. Gyulassy, Nucl. Phys. A **608**, 479 (1996).

[172] D. Peressounko, Phys. Rev. C **67**, 014905 (2003).

[173] E. Frodermann, U. Heinz, Phys. Rev. C **80** 044903 (2009).

[174] J. Alam, B. Mohanty, P. Roy, S. Sarkar and B. Sinha Phys. Rev. C **67**, 054902 (2003).

[175] S. A. Bass, B. Mueller and D. K. Srivastava, Phys. Rev. Lett. **93**, 162301 (2004).

[176] D. K. Srivastava and J. I. Kapusta, Phys. Lett. **B319**, 407 (1993); D. K. Srivastava, Phys. Rev. D **49**, 4523 (1994).

[177] D. K. Srivastava and R. Chatterjee, Phys. Rev. C **80**, 054914 (2009).

[178] P. Mohanty, J. K. Nayak, J. Alam and S. K. Das, Phys. Rev. C **82** 034901 (2010).

[179] P. Mohanty, J. Alam and B. Mohanty, Phys. Rev. C **84**, 024903 (2011);

[180] P. Mohanty, J. Alam and B. Mohanty, Nucl. Phys. A **862** 301-303, (2011).

[181] D. H. Rischke and M. Gyulassy, Nucl. Phys. A **608**, 479 (1996).

[182] M. Herrmann and G. F. Bertsch, Phys. Rev. C **51**, 328 (1995).

[183] S. Chappman, P. Scotto and U. Heinz, Phys. Rev. Lett. **74**, 4400 (1995).

[184] K. Kajantie, and P. V. Ruuskanen, Phys. Lett. **121**,352 (1983).

[185] C. Y. Wong and H. Wang, Phys. Rev. **C 58**, 376 (1998).

[186] L. D. McLerran and T. Toimela, Phys. Rev. D **31**, 545 (1985).

[187] C. Gale and J.I. Kapusta, Nucl. Phys. B **357**, 65 (1991).

[188] J. Alam, S. Raha and B. Sinha, Phys. Rep. **273**, 243 (1996).

[189] C. Bernard *et al.*, Phys. Rev. D **75** 094505 (2007).

[190] B. Mohanty and J. Alam, Phys. Rev. C **68**, 064903 (2003).

[191] M. Asakawa and T. Hatsuda, Phys. ReV. D **55**, 4488 (1997).

[192] Y. Akamatsu, and N. Yamamto, Phys. Rev. Lett. **111**, 05202 (2013).

[193] M. Strickland, Acta Phys. Pola. B **45**, 2355 (2014).

Appendix A

Relation between the dielectric tensor and the self-energy in anisotropic QGP

The spatial component of induced current density is given by (see Eq. (3.27)),

$$\begin{aligned} J^i_{ind}(K) &= g^2 \int_{\mathbf{p}} V^i \partial^l_{(p)} f(\mathbf{p}) \mathcal{M}_{jl}(K,V) D^{-1}(K,\mathbf{v},\nu) A^j(K) + 2N_c g \nu \mathcal{S}^g(K,\nu) \\ &+ g^2(i\nu) \int \frac{d\Omega}{4\pi} V^i D^{-1}(K,\mathbf{v},\nu) \int_{\mathbf{p}'} \partial^l_{p'} f(\mathbf{p}') \mathcal{M}_{jl}(K,V') D^{-1}(K,\mathbf{v}',\nu) \mathcal{W}^{-1}(K,\nu) A^j(K) \\ &+ 2N_c g^2 (i\nu^2) \int \frac{d\Omega}{4\pi} V^i D^{-1}(K,\mathbf{v},\nu) \mathcal{S}^g(K,\nu) \mathcal{W}(K,\nu). \end{aligned} \tag{A.1}$$

The spatial component of the polarization tensor can be written from Eq. (3.29) as:

$$\begin{aligned} \Pi^{ij}(K) &= g^2 \int_{\mathbf{p}} V^i \partial^l_{(p)} f(\mathbf{p}) \mathcal{M}_{jl}(K,V) D^{-1}(K,\mathbf{v},\nu) \\ &+ g^2(i\nu) \int \frac{d\Omega}{4\pi} V^i D^{-1}(K,\mathbf{v},\nu) \\ &\times \int_{\mathbf{p}'} \partial^l_{p'} f(\mathbf{p}') \mathcal{M}_{jl}(K,V') D^{-1}(K,\mathbf{v}',\nu) \mathcal{W}^{-1}(K,\nu) \end{aligned} \tag{A.2}$$

We also note that the thermal conductivity and the dielectric tensor is related by [125]

$$\epsilon^{ij}(K) = \delta^{ij} + \frac{i}{\omega} \sigma^{ij}(K) \tag{A.3}$$

where $\sigma^{ij}(K) = \frac{\delta J^i_{ind}(K)}{\delta E_j(K)}$ Using Eq. A.1 we derive

$$\begin{aligned} \sigma^{ij}(K) &= \frac{ig^2}{\omega} \Bigg[\int_{\mathbf{p}} V^i \partial^l_{(p)} f(\mathbf{p}) \mathcal{M}_{jl}(K,V) D^{-1}(K,\mathbf{v},\nu) + i\nu \int \frac{d\Omega}{4\pi} V^i D^{-1}(K,\mathbf{v},\nu) \\ &\times \int_{\mathbf{p}'} \partial^l_{p'} f(\mathbf{p}') \mathcal{M}_{jl}(K,V') D^{-1}(K,\mathbf{v}',\nu) \mathcal{W}^{-1}(K,\nu) \Bigg] \end{aligned} \tag{A.4}$$

Here we have use the following relations in temporal axial gauge:

$$E_i = F_{0i} = \partial_0 A_i - \partial_i A_0 = -i\omega A_i. \tag{A.5}$$

Using the above relations it is straightforward to show that

$$\epsilon^{ij}(K) = \delta^{ij} - \frac{\Pi^{ij}(K)}{\omega^2}. \tag{A.6}$$

• ○ •

Appendix B

Analytic expression for structure functions in static limit

In the limit $\omega \to 0$, all four structure functions can be done analytically. We can define four mass scales

$$\begin{aligned} m_\alpha^2 &= \lim_{\omega\to 0} \alpha, \\ m_\beta^2 &= \lim_{\omega\to 0} -\frac{q^2}{\omega^2}\beta, \\ m_\gamma^2 &= \lim_{\omega\to 0} \gamma, \\ m_\delta^2 &= \lim_{\omega\to 0} \frac{\widetilde{n}q^2}{\omega} \operatorname{Im}\delta \end{aligned} \tag{B.1}$$

The results for

$$\begin{aligned} m_\alpha^2 &= -\frac{m_D^2}{2q_x^2\sqrt{\xi}}\left(q_z^2 \arctan\sqrt{\xi} - \frac{q_z q^2}{\sqrt{q^2+\xi q_z^2}} \arctan(\frac{\sqrt{\xi}q_z}{\sqrt{q^2+\xi q_z^2}})\right) \\ m_\beta^2 &= m_D^2 \frac{(\sqrt{\xi}(1+\xi)\arctan\sqrt{\xi})(q^2+\xi q_x^2) + \xi q_z(q_z\sqrt{\xi} + \frac{q^2(1+\xi)}{q^2+\xi q_x^2}\arctan\frac{\xi q_z}{\sqrt{q^2+\xi q_x^2}})}{2\sqrt{\xi}(1+\xi)(q^2+\xi q_x^2)} \\ m_\gamma^2 &= -\frac{m_D^2}{2}\left(\frac{q^2}{q^2+\xi q_x^2} - \frac{1+2q_z^2/q_x^2}{\sqrt{\xi}}\arctan\sqrt{\xi}\right. \\ &+ \left.\frac{q^2 q_z(2q^2+3\xi q_x^2)}{\sqrt{\xi}(q^2+\xi q_x^2)^{3/2}q_x^2}\arctan\frac{\sqrt{\xi}q_z}{\sqrt{q^2+\xi q_x^2}}\right) \\ m_\delta^2 &= -\frac{\pi m_D^2 \xi q_x q_z q}{4(q^2+\xi q_x^2)^{3/2}} \end{aligned} \tag{B.2}$$